Refractoriness of Cardiac Muscle as Affected by Intercalated Disks: A Model Study Implications for Fibrillation and Defibrillation

H. G. Haas[1] and K. Solchenbach[2]

[1] *Department of Physiology, University of Bonn, Bonn, Germany*
[2] *Pallas GmbH, Bruehl, Germany*

Abstract. It is generally agreed that inhomogeneities of the recovery process in cardiac tissue play an important role in the genesis of reentrant arrhythmias. Regarding cardiac muscle as an assembly of discrete cells connected by gap junctions, differences in recovery may result from a nonuniformity of membrane or cable properties. In this study, a computer model of a one-dimensional cardiac muscle fiber including a periodic intercalated disk structure is used to study the influence of disk resistance (R_j) and stimulus strength (J) on refractoriness. Stimulating currents are applied externally in a bipolar arrangement. The basic effect of a current pulse is local de- and hyperpolarizations at the ends of an individual cell. Polarization develops very rapidly and increases with increasing values of R_j or J so that an interaction with membrane current kinetics becomes possible. When a premature stimulus is applied during repolarization of a conditioning action potential, multiple Na currents can occur, either caused by depolarization of the cathodal end of a cell or in the form of anode break excitation at the hyperpolarized end. Those currents affect the response of a fiber such that, at a given value of J, the refractory period is shortened by an increase in R_j. In a ring fiber model with different R_j values in the two halves of ring an extrastimulus timed between the refractory periods of the two branches results in a sustained circus movement. Varying stimulus strength yields an upper limit of vulnerability characterized by a "synchronized extrasystole". The ring model also implies the suppression of circus movement by an external shock. The minimal shock strength required for suppression is close to the upper limit of vulnerability. The simulations suggest that discrete effects of junctional resistance may be involved in fibrillation and defibrillation.

Key words: Cardiac muscle — Disk resistance — Computer simulation — Refractoriness — Circus movement

Correspondence to: H. G. Haas, Department of Physiology, University of Bonn, 31 Wilhelm St., 53111 Bonn, Germany

Introduction

The problem of intercellular communication in organized tissues has been of growing interest during the past decades. In excitable tissues, e.g. cardiac or smooth muscle, a mode of signal transmission between adjacent cells is required for propagation of the electrical impulse. It is widely accepted that intercellular coupling is brought about by specialized membrane structures (gap junctions) allowing local circuit current generated in a cell to enter a neighbouring cell without penetrating the extracellular space.

In mammalian heart muscle, gap junctions are concentrated in the intercalated disks forming an end-to-end contact between adjacent cells, but lateral nexus structures are also present. From an electrophysiological viewpoint, the basic effect of intercalated disks is an impediment to axial current flow. Thus, the disks may affect the distribution of a stimulating current in cardiac tissue and the polarizing effects due to current flow. This is best seen in the case of an external field stimulation. When a current is applied to a fiber *via* extracellular electrodes placed at the fiber ends, the current will distribute between the extra- and the intracellular space. If we think of the cells as little cylinders aligned in a chain, the intracellular current will produce a voltage jump at every cellular junction. This effect was referred to as the sawtooth effect (cf. the model studies of Plonsey and Barr 1986a,b; Plonsey et al. 1991; Cartee and Plonsey 1992). It implies a polarization of the individual cells, with a hyperpolarization at the cell end facing the anode and a depolarization at the other end, which superimposes to the overall polarization of the fiber as a whole. The sawtooth effect has not been demonstrated experimentally as yet, possibly because the electrical and optical recording techniques available at present lack the necessary spatial resolution. However, the effect is well-founded on theoretical considerations as a simple consequence of Ohm's law. The larger the disk resistance or the stimulus strength (J), the more pronounced will be the polarizing effect at the cellular junctions. With strong stimulating currents, like those used for cardiac defibrillation, the transmembrane potential changes induced in the individual cells may be large enough to interfere with the kinetics of membrane ionic currents, so that initiation and propagation of an electrical impulse can be essentially different from the behavior of a continuous fiber.

In this article, a one-dimensional computer model of a cardiac fiber is used to study the effects of intercalated disks under conditions of external field stimulation. The model is designed to represent an excised cardiac strand enveloped by a thin sheet of interstitial fluid. The focus of the study is on possible variations of the refractory behavior when premature stimuli of different strength are applied under different degrees of cell-to-cell coupling. The simulations show a complex interaction of stimulus strength (J) and junctional resistance (R_j) in the generation of refractory phenomena. In a restricted range of rather low stimuli and low R_j, the refractory period is shortened by an increase in J (as expected from the classical strength-interval relation) but is also shortened by an increase in R_j. When higher values of J and R_j are considered, a clear definition of the refractory period is lost.

Furthermore, the conduction velocity of an extrasystole increases with increasing J, tending to a synchronization of the signal in the central portion of the fiber. These effects are mainly due to an occurrence of extra Na currents induced by the sawtooth mechanism. When switching from a linear to a ring-shaped structure, vulnerability phenomena can be demonstrated. For this we use a ring model with different values of R_j in the two halves of ring, resulting in a difference in refractory period duration. Stimulating electrodes are positioned at the boundaries between the two segments. Under these conditions, generation as well as suppression of circus movement are observed.

Materials and Methods

In this paper, the electrical responses of linear and ring-like structures of cardiac tissue are considered. Both structures are represented by a discontinuous model of serially arranged cells.

The theoretical fiber consists of 15–400 cylindrical cells (each 200 μm in length and 28 μm in diameter) joined end-to-end by gap junctions and is surrounded by a restricted extracellular space. The ratio of extra- and intracellular space is taken to be $1:3$. It is assumed that both pathways carry longitudinal current only. The core conductor model is used to describe the impulse propagation over a cell.

Five components of membrane ionic current are incorporated in the model:
1. Fast Na current, I_{Na}, of the Hodgkin and Huxley (1952a,b) type with maximum Na conductance $\overline{g_{\mathrm{Na}}} = 35$ mS/cm^2 and $E_{\mathrm{Na}} = 50$ mV. The rate constants of activation and inactivation are defined by

$$\alpha_m = 0.1(V+49)/\{1-\exp[-0.1(V+49)]\} \qquad \alpha_h = 0.07\exp[-0.2(V+79)]$$
$$\beta_m = 4\exp[-(V+74)/18] \qquad \beta_h = 1/\{1+\exp[-0.1(V+50)]\}$$

where the membrane potential V is expressed in mV and the dimension of α, β is ms^{-1}.
2. Ca current is defined as a unidirectional Ca influx

$$I_{\mathrm{Ca}} = -df\{4P_{\mathrm{Ca}} \cdot F[\mathrm{Ca}]_{\mathrm{o}} \cdot VF/RT\}/[\exp(2VF/RT) - 1]$$

where the bracketed terms mean the fully activated (steady) current. With $P_{\mathrm{Ca}} = 11.5 \times 10^{-6}$ cm/s, $F = 96,500$ Coul/mol and $[\mathrm{Ca}]_{\mathrm{o}} = 1.8$ mmol/l the term $4P_{\mathrm{Ca}} \cdot F \cdot [\mathrm{Ca}]_{\mathrm{o}}$ comes to 8 μA/cm^2. The gating kinetics of d and f is described by

$$\alpha_{\mathrm{d}} = 0.03(V+5)/\{1-\exp[-0.25(V+5)]\}$$
$$\alpha_f = 0.00625(V+15)/\{\exp[0.25(V+15)]-1\}$$
$$\beta_{\mathrm{d}} = 0.012(V+5)/\{\exp[0.1(V+5)]-1\}$$
$$\beta_f = 0.05/\{1+\exp[-0.25(V+15)]\}$$

3. Hyperpolarizing-activated current, I_f (DiFrancesco and Noble 1985). The related channels are thought to pass Na^+ and K^+ with approximately equal conductances.

With $E_{\mathrm{Na}} = 50$, $E_{\mathrm{K}} = -90$ mV the reversal potential of this current is at -20 mV. We use the formulation

$$I_f = y\overline{g_f}\,[(V - E_{\mathrm{Na}}) + (V - E_{\mathrm{K}})]$$

where $\overline{g_f}$ is set to 0.0159 mS/cm^2 and y is an activation variable defined by the rate constants

$$\alpha_y = 2.5 \cdot 10^{-5} \exp[-0.067(V + 52)]$$
$$\beta_y = 5 \cdot 10^{-4}(V + 52)/\{1 - \exp[-0.2(V + 52)]\}$$

4. Time-dependent (delayed) K^+ current, I_{K}. This current is also considered as a "mixed" one but the contribution of Na^+ is probably small so that the reversal potential is around -80 mV. A typical feature of this current is an inward-going rectification near the resting potential. Adopting a formulation similar to that proposed by DiFrancesco and Noble (1985) the current (in μA/cm^2) may be described by

$$I_{\mathrm{K}} = x \cdot 2.7[1 - 0.043 \exp(-V/25)]$$

The variable x obeys a first-order kinetics with the rate constants

$$\alpha_x = 5 \cdot 10^{-4} \exp[0.0826(V + 50)]/\{1 + \exp[0.057(V + 50)]\}$$
$$\beta_x = 1.3 \cdot 10^{-3} \exp[-0.06(V + 20)]/\{1 + \exp[-0.04(V + 20)]\}$$

5. Time-independent current, I_{K_1}, which is considered as a pure K current:

$$I_{\mathrm{K}_1} = 1.667(V - E_{\mathrm{K}})/\{1 + \exp[(V + 100)/13]\}$$

Fig. 1A illustrates the electrical equivalent circuit used for computation of signal propagation along a discontinuous fiber. Neighbouring cells are connected by gap junctions. Stimulating current (I) is applied in a manner simulating longitudinal field stimulation. The basic equation for the membrane potential (V) as function of x and t is

$$\partial^2 V/\partial x^2 = (r_{\mathrm{o}} + r_i)(c_m \partial V/\partial t + i_{\mathrm{ion}}) \tag{1}$$

Implying sealed ends of the fiber the boundary condition at $x = 0$ and $x = L$ is $\partial V/\partial x = r_{\mathrm{o}} I$. The initial condition is $V = V_r$ all along the fiber. $V(x, t)$ is a continuous function within each cell but discontinuities arise at the cell junctions. Gap junctions are taken as purely resistive elements. Since the width of a junctional region is very small compared to the cell length (R_j) may be treated as a spatial delta function. This means that the internal potential (φ_i) undergoes a jump $\Delta\varphi_i = -i_i R_j$ at any junction and the same is true for the membrane potential $V = \varphi_i - \varphi_{\mathrm{o}}$ because the external potential (φ_{o}) is a continuous function of x.

The ring model (Fig. 1B) used in this study is obtained by connecting the edges of a one-dimensional fiber. Stimulus current I is applied between two extracellular

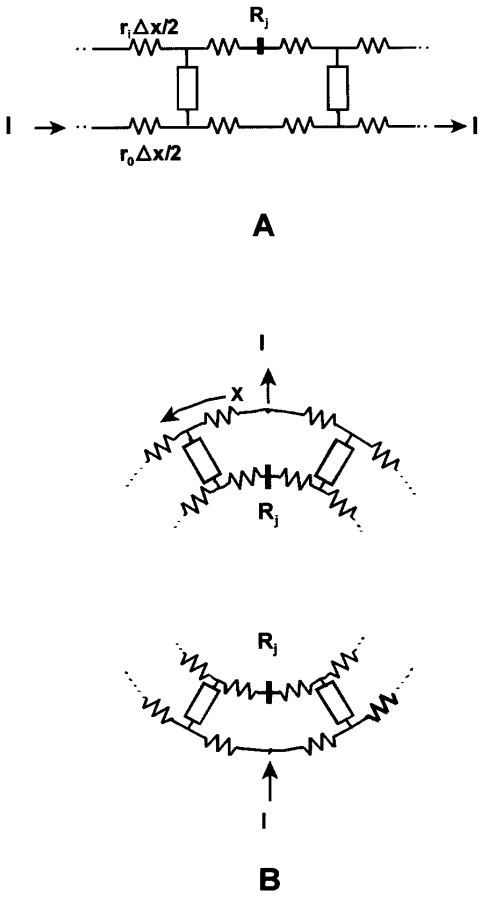

Figure 1. Network models used for simulation. **A.** Discrete cable model of a cardiac fiber (for parameter values see Table 1). Cells are coupled by an intercalated disk structure. The disk resistance, R_j, represents the effective axial resistance of the gap junctional channels and is marked by a vertical bar. Extra- and intracellular fluids are represented by passive lumped resistors. Each individual cell is discretized into N_x membrane patches. The open box is a symbol for membrane capacitive and ionic current flow. External stimulus (DC) current, I, is applied in a bipolar arrangement with the cathode at the left end ($x = 0$) and the anode at the right end ($x = L$) of the fiber. Stimulus duration is 0.5 ms throughout the study unless otherwise stated. In the simulations, stimulus strength is noted as current density (J) referred to the cross-section of the fiber (8.04×10^{-6} cm^2). **B.** Discrete model of a ring-shaped structure consisting of up to 400 cells, each 200 μm in length. Stimulus current is injected at the bottom of ring and leaves the network at the top. Distance x is taken in anticlockwise direction, with the origin at the top of ring (cathode).

sites which are located in diametrical opposition. Current injected at the anode (bottom of ring) distributes on the two branches according to

$$I = i_{\mathrm{o}}^{r} - i_{\mathrm{o}}^{l} = -r_{\mathrm{o}}(\partial\varphi_{\mathrm{o}}^{r}/\partial x - \partial\varphi_{\mathrm{o}}^{l}/\partial x) \tag{2}$$

where the superscripts r and l refer to the right and the left branch, respectively, and the derivatives are taken unidirectionally. A further condition is that the internal voltage drops resulting from current flow through the myoplasm and the disks sum up to zero when the ring is considered as a whole. The fiber parameters are summarized in Table 1.

Computational methods: the simulation system solves the cable equation (1) for the whole fiber and couples to it the ODEs (in time) for the reaction variables m, h, d, f, y, and x. Each cell is discretized by N_x equidistant grid-points. For short fibers consisting of 15 cells we use $N_x = 9$, for long fibers of 400 cells

Table 1. Simulation parameters

Fixed quantities are:		
Cell length, d	0.02	cm
Cell radius, a	0.0014	cm
Fiber (extra- plus intracellular space) radius, b	0.0016	cm
Extracellular resistivity, ρ_o	60	$\Omega \cdot$ cm
External resistance *per* unit of fiber length, $r_o = \rho_o/\pi(b^2 - a^2)$	31.83	$M\Omega \cdot cm^{-1}$
Intracellular resistivity, ρ_i	200	$\Omega \cdot$ cm
Internal resistance *per* unit length, $r_i = \rho_i/\pi a^2$	32.48	$M\Omega \cdot cm^{-1}$
Membrane capacitance, C_m	2	$\mu F \cdot cm^{-2}$
Membrane capacitance *per* unit length, $c_m = C_m 2\pi a$	0.0176	$\mu F \cdot cm^{-1}$
Resting membrane potential, V_r	−85.2	mV
Specific membrane resistance (resting value), R_m	2.78	$k\Omega \cdot cm^2$
Membrane resistance *per* unit length, $r_m = R_m/2\pi a$	316	$k\Omega \cdot$ cm
Membrane time constant, τ_m	5.56	ms
Space constant, $\lambda = [r_m/(r_o + r_i)]^{1/2}$	0.071	cm
Disk resistance, R_j	0–10	MΩ
Variable quantities are:		
Transmembrane (inside minus outside) potential, V (mV)		
Membrane current *per* unit length, i_m (μA/cm)		
Ionic current *per* unit length, i_{ion} (μA/cm)		
Stimulating current, I (mA)		
Stimulating current density (referred to cross-section of fiber), $J = I/\pi b^2 = I/8.04 \times 10^{-6}$ (mA/cm^2)		
Axial (internal) current, i_i (μA)		
External current, i_o (μA)		

we take $N_x = 3$. The discretization in time is fully implicit so that no stability restriction on the time-step size implies. In each time-step a nonlinear system of equations is solved by a Newton–Raphson method. The step size for time integration is chosen automatically preserving a predefined local accuracy. The program and the discretization have been validated and convergence of the results has been demonstrated. The program was written in Fortran, the runs were executed on a Sun workstation. Data and graphs were processed with MS-Excel.

Results

Section A. Polarizing effects of disk resistance R_j

Fig. 2 demonstrates the variation of membrane potential along a 15 cell length equivalent cable shortly after onset of a DC field stimulation. Obviously, a few hundredths of ms are sufficient to produce a typical sawtooth pattern, with a potential jump at each cell junction. The jumps simply reflect the voltage drop across a junction, $-i_i R_j$ (Plonsey and Barr 1986a,b). In the central region of the cable the voltage pattern is quasi-periodic and polarization of an interior cell is

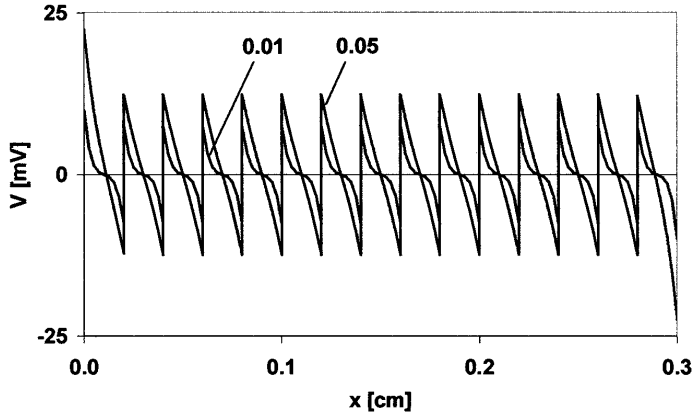

Figure 2. Voltage responses of a 15 cell chain (passive membrane, $R_j = 1$ MΩ) to a rectangular current pulse (-12.1 mA/cm^2) of 0.01 or 0.05 ms duration, respectively. Resting potential is set to zero level.

antisymmetric to the cell's midpoint. Thus, each cell – not only the cable as a whole – shows a cathodal and an anodal effect, i.e., a depolarization at one end of the cell and a hyperpolarization of the same size at the other end. Cellular polarization develops much faster than it is expected from the membrane time constant (in our model 5.56 ms) and is about 95% complete at $t = 0.03$ ms (Krassowska et al. 1990; see also Appendix).

Quantitatively, the full polarization of an interior cell may be described by

$$V(\xi) = \frac{I r_o R_j}{2(r_o + r_i)} \; \frac{\sinh(\xi/\lambda)}{\sinh(\mathrm{d}/2\lambda) + [R_j/2\lambda(r_o + r_i)]\cosh(\mathrm{d}/2\lambda)} \tag{3}$$

where the cell's midpoint is chosen as the origin of the axial co-ordinate ξ. Using the parameter values (r_o, r_i, d, λ) listed in Table 1 and setting R_j to 0.33, 1, 3, and 5 MΩ an applied current $I = 0.1$ μA (corresponding to a longitudinal current density of 12.4 mA/cm^2) will polarize the ends of an interior cell ($\xi = \pm \mathrm{d}/2$) by 6.5, 13.9, 22.2, and 25.2 mV, respectively. Those figures characterize the size of the polarizing effect.

The above simulations refer to structures with linear membrane characteristics. In a fiber endowed with excitable membranes similar polarizing effects due to external current application are expected. If polarization of the individual cells is large enough, the local de- and hyperpolarizations may interfere with the kinetics of membrane ionic currents, thereby affecting initiation and propagation of an action potential.

A major point is the generation of multiple Na currents by the sawtooth pattern. Such an effect is expected when the depolarizing spike at the left (cathodal) end of an interior cell reaches, or exceeds, the threshold potential for Na current

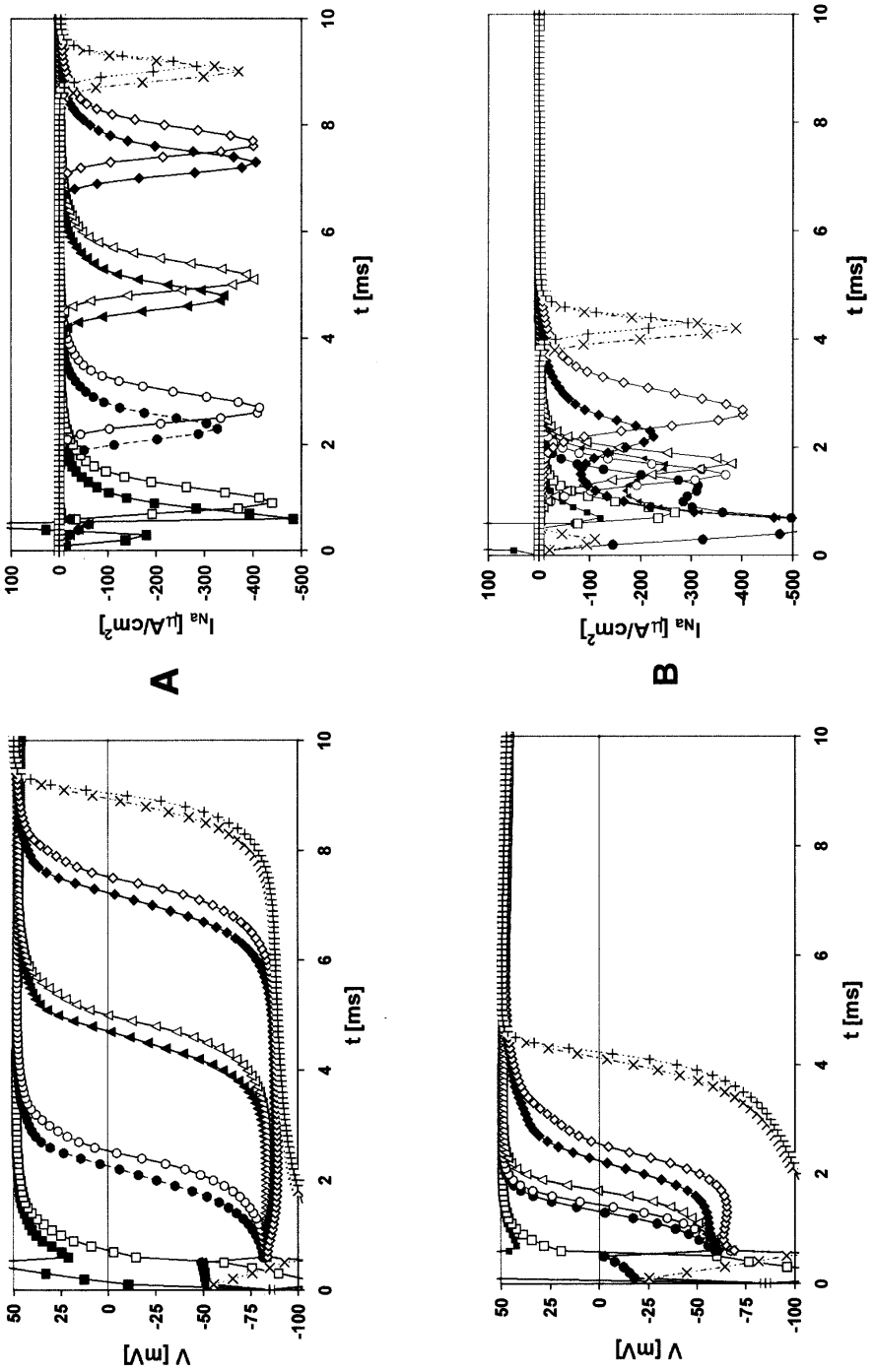
A
B
I_{Na} [µA/cm²]
V [mV]
t [ms]

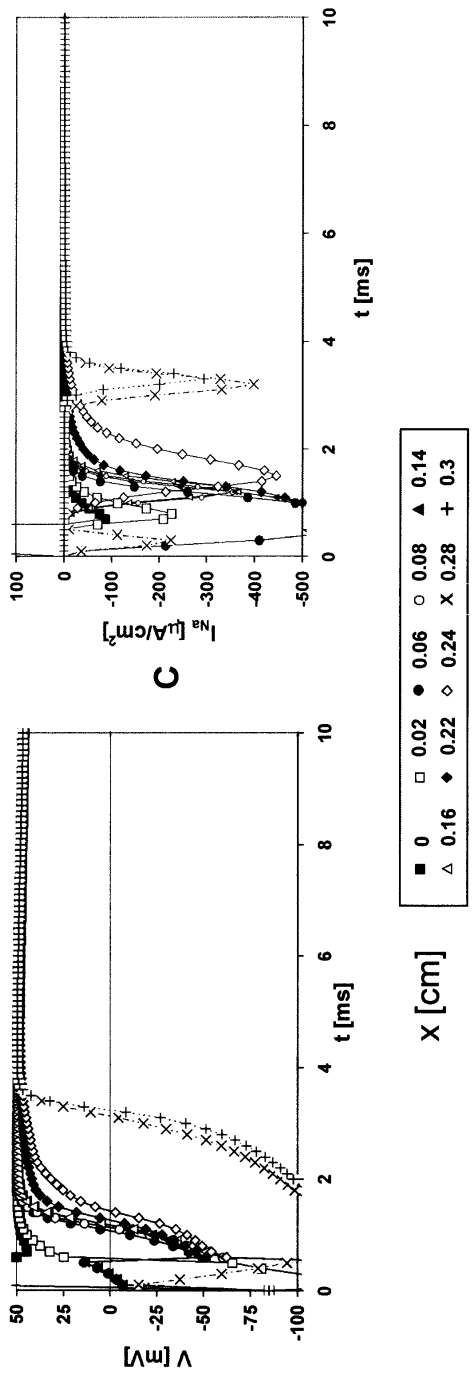

Figure 3. Conduction velocity as affected by stimulus strength. Records of membrane potential and Na current from a theoretical 15 cell fiber with $R_j = 1$ MΩ, using stimulating currents of −30 (A), −60 (B), and −70 mA/cm^2 (C). The plots show the rising phase of the action potential and the time course of Na current at both ends of cells 1, 4, 8, 12, and 15, distinguished by different symbols. Note the occurrence of two Na currents in succession in the interior cells (4–12) with stronger stimuli. The immediate currents (related to the depolarizing spikes of the sawtooth effect) are superimposed to give an almost uniform deflection. Formally, an increase in conduction velocity appears as a "compression" of action potential contours over the interior cells.

activation. This is the case with higher values of J or R_j. Fig. 3 illustrates the effect of increasing J at a given value of disk resistance. With a low stimulus current (Fig. 3A), action potential propagation and occurrence of Na currents are continuously interrelated, resembling the behavior of a continuous fiber. When the stimulating current is doubled, the situation is more complex (Fig. 3B): the interior cells of the fiber produce large Na currents immediately after onset of stimulation. These currents are restricted to the left (depolarized) half of a cell and are a direct consequence of the local depolarizations caused by the sawtooth effect. All these currents are similar in size and shape and occur almost simultaneously. Thus we have two Na currents in succession: the first one as an immediate effect of stimulation (shown at the left edge of the current plots in Fig. 3B) and the second one associated with signal propagation along the fiber. The excess of Na current leads to an increase of axial current i_i which in turn increases conduction velocity. With even stronger stimuli (not shown), the immediate Na currents will be large enough to activate the interior cells directly, that is: at the same time (Krassowska et al. 1992). In the following the term "synchronization" will be used to describe this phenomenon. (The term is, of course, to be understood as an approximation rather than in a strict sense.)

Synchronization is a typical inference from the sawtooth effect. In principle, synchronization is seen with any $R_j > 0$ provided that stimuli of sufficient strength are applied. The higher the R_j value, the lower is the stimulus requirement for this phenomenon. Fig. 4 illustrates the general configuration of conduction velocity,

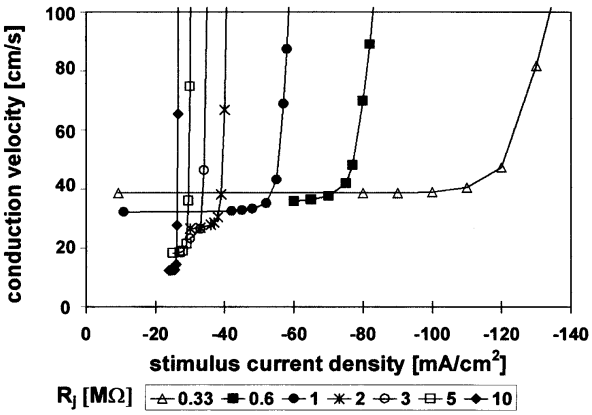

Figure 4. Conduction velocity as function of R_j and J. Data were derived from action potential propagation between cells 4 and 12 of a 15 cell fiber, stimulated by short (0.5 ms) current pulses of varying intensity. The plots represent the relations between average velocity and stimulus strength for junctional resistances ranging from 0.33 to 10 MΩ. Each plot consists of a horizontal section and an ascending limb. Starting point of the horizontal section corresponds the respective diastolic threshold value (explicitly shown for $R_j = 0.33$ and 1 MΩ).

stimulus strength, and junctional resistance. The plots characterize the strength-velocity relations at different values of R_j. Each plot begins with a horizontal line, corresponding to a range where average velocity is almost independent of stimulus strength. It follows a region where velocity increases with increasing strength: first slowly, then in an almost exponential fashion, tending to a "synchronization" of the excitation process in the interior cells of the fiber. The higher R_j, the shorter is the horizontal part of a plot and the steeper is the ascending limb.

Section B. Disk resistance effects on refractoriness

When an action potential has been elicited in a cardiac muscle cell, reexcitation will not be possible until repolarization has reached a certain level. Assuming a uniform polarization of the membrane, the refractory behavior may be interpreted in terms of membrane ionic properties. In this connection, the availability of the Na system, characterized by the inactivation variable h, is the most important parameter. The situation is more complex in a multicellular preparation, e.g. a cable-like structure where excitation spreads with a relatively low speed. Using stimuli of a given strength, the "functional" refractory period may be defined by the earliest moment of recovery when it becomes possible to evoke a new propagated action potential by an extrastimulus of that strength (Hoffman and Cranefield 1960; Antoni 1992). In general, the refractory behavior does not only depend on membrane parameters but also on cable properties. Thus, an effect of disk resistance on refractory phenomena may be expected.

To investigate this problem in our model, we used a two-pulse arrangement similar to that used in experimental studies: a conditioning (basic) action potential was elicited by a current pulse J_1 at time $t_1 = 0$ and a second pulse (extrastimulus) J_2 was applied at various times t_2 during repolarization of the conditioning action potential. Both stimuli were applied through extracellular electrodes as shown in Fig. 1A.

A simple example for an effect of R_j on the refractory behavior is given in Fig. 5 where a continuous and a discontinuous fiber with same dimensions and same membrane properties are compared. Both fibers are subjected to the same extrastimulus (J_2) at the same time (t_2). While the fiber with the high disk resistance (B) produces a new regenerative signal, the continuous fiber (A) fails to do so. Thus, the refractory period of the discontinuous fiber appears to be shortened. It should be noted that this effect cannot be explained in terms of Na channel availability because repolarization of the basic action potential in (B) is slightly delayed compared to (A) so that at the time of premature stimulation the value of h is higher in (A) than in (B). Rather it seems that the interplay between excitatory Na current, axial current flow, and polarization of the downstream membrane is altered by the presence of recurrent discontinuities of internal resistance and that those alterations give rise to changes in the refractory behavior. In the following this problem is considered in more detail.

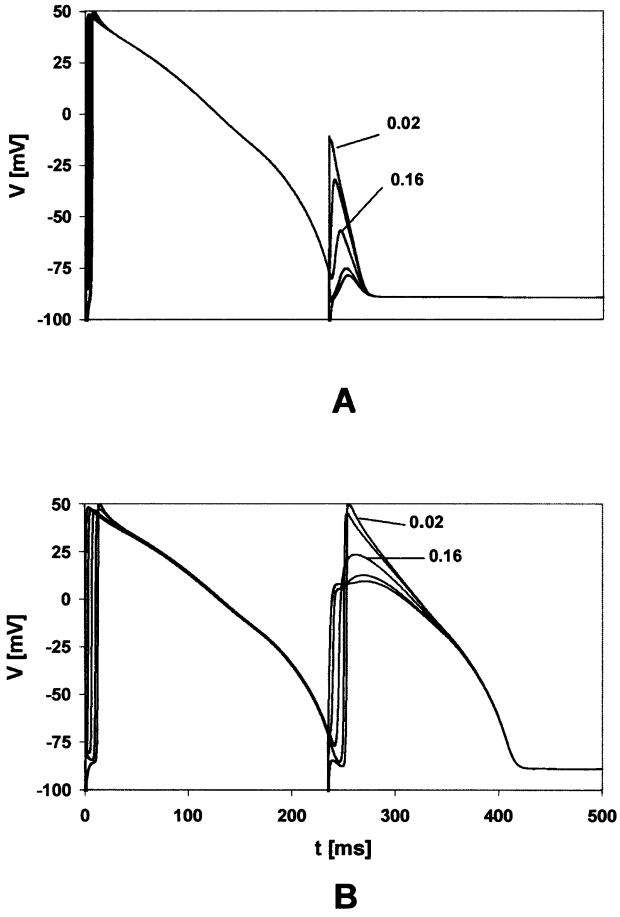

Figure 5. Influence of disk resistance on refractoriness. Comparison between a continuous fiber ($R_j = 0$; A) and a discontinuous fiber ($R_j = 3$ MΩ; B) of length 0.3 cm (15 cells). Two current pulses (-25 mA/cm^2; 0.5 ms) are applied at an interval of 235 ms. The voltage response to the second pulse is a decremental wave in (A) and a new action potential in (B).

1. Different types of responses to premature stimuli

In general, the response of a discontinuous fiber to an extrastimulus will depend on the size of R_j, J_2, and the time of application (t_2). To get a synopsis of possible effects, the model of a short (15 cell) fiber with normal or elevated R_j was used and the voltage and current responses to premature stimuli of varying intensity were tested. In any case, the immediate effect of the stimulus is a zigzag-like distortion of the voltage profile existing just prior to stimulus incidence. Each cell is depolarized

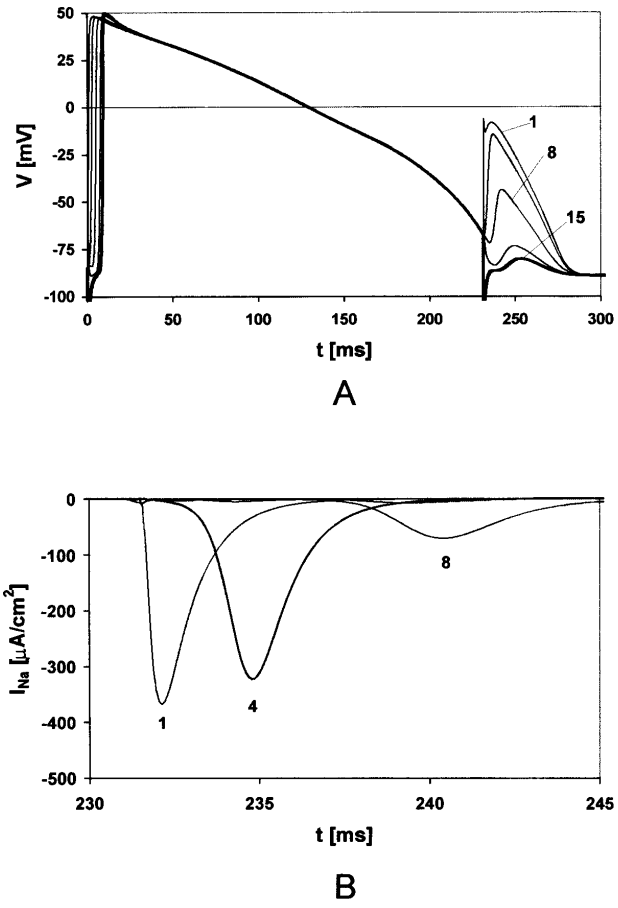

Figure 6. Two-pulse stimulation of a discontinuous 15 cell fiber with $R_j = 1$ MΩ; $J_1 = -25$, $J_2 = -32.4$ mA/cm^2; pulse duration 0.5 ms; $t_2 = 231$ ms. **A.** Voltage responses on a large time scale. Records refer to the right (anodal) end of cells 1, 4, 8, 12, 15. **B.** Na currents associated with the premature stimulus. Currents are restricted to the left (cathodal) half of the fiber and arise from the right (anodal) end of the cells.

at the left (cathodal) end and hyperpolarized at the right end. In principle, this is the same effect as shown in Fig. 2. The question, then, is to which extent the local polarizations will interfere with the kinetics of membrane currents, in particular the Na system.

The reaction of the fiber is best studied with moderate values of R_j and J_2. In a series of simulations we set R_j to 3 times its normal value and J_2 to 3 times the diastolic threshold value. A systematic variation of t_2 led to the following results:

When the extrastimulus is applied during the plateau phase of the conditioning action potential (e.g. $t_2 = 200$ ms), the effect is simply an *action potential prolongation*. The depolarizing spikes of the sawtooth pattern may reach, or exceed, the zero potential level. However, as the recovery of the Na system is very small at the time of stimulation the spikes fail to produce any significant Na current.

When J_2 is applied during the final phase of repolarization, the voltage responses change distinctly and now appear as *decremental wave* attached to the end of the conditioning action potential. Fig. 6A illustrates the effect observed with $t_2 = 231$ ms. In this case excitatory Na currents are observed but these currents are typically restricted to the right (anodal) end of a cell which had been hyperpolarized by the stimulus (Fig. 6B). We consider these currents as caused by an anodal break effect. To verify this assumption we modified the two-pulse protocol used in Fig. 6 by using premature stimuli of longer duration (1, 2, or 3 ms). Fig. 7 illustrates the anodal effect of a 2-ms pulse on an interior cell. It is clearly seen that a Na current develops with a latency which tightly fits the stimulus duration. This supports the idea of an anode break mechanism. The "driving force" for the Na current is delivered by the depolarization associated with the conditioning action potential.

When the stimulus is applied 1 ms later ($t_2 = 232$ ms), the situation changes abruptly (Fig. 8). Now, the voltage response is a new *propagated action potential* (an extrasystole) which shows some irregularities (notches and dips) in the rising phase (Fig. 8A). Excitatory Na currents are of different origin. Membrane potential just prior to the stimulus is ~ -72 mV and the availability of the Na system is still very small. Thus, the depolarizing spikes of the sawtooth pattern do not produce any marked Na current. The current pattern is dominated by Na currents arising from the right (anodal) end of the cells (Fig. 8B). When the wave enters the right half of the fiber, Na currents also occur at the left end of a cell as a secondary effect. With further delay of stimulation, the distortions of the rising phase disappear and the contour of the new signal comes to be completely smooth. Na currents now occur all along the fiber but are still accentuated at the right (anodal) end of each cell (not shown). Full recovery is not seen until stimulus delay is 350 ms or more, i.e., recovery lags behind repolarization.

In the above analysis, three types of voltage responses to a premature stimulus are clearly distinguished, depending on the time of stimulus incidence. There is a rather long period ("interphase"), from 207 to 231 ms, where stimulation causes a signal with decremental conduction. Before and after that period, the voltage response is nondecremental in nature: either a prolongation of the basic action potential or the generation of a new action potential. The end of the interphase may be taken to characterize the duration of the functional refractory period. In the case of a discontinuous fiber illustrated in Figs. 6 and 8, the refractory period comes to about 232 ms. In a continuous fiber with same dimensions and same membrane properties, the refractory period lasts about 236 ms. Thus, restoration of excitability seems to be favored by the presence of intercalated disks.

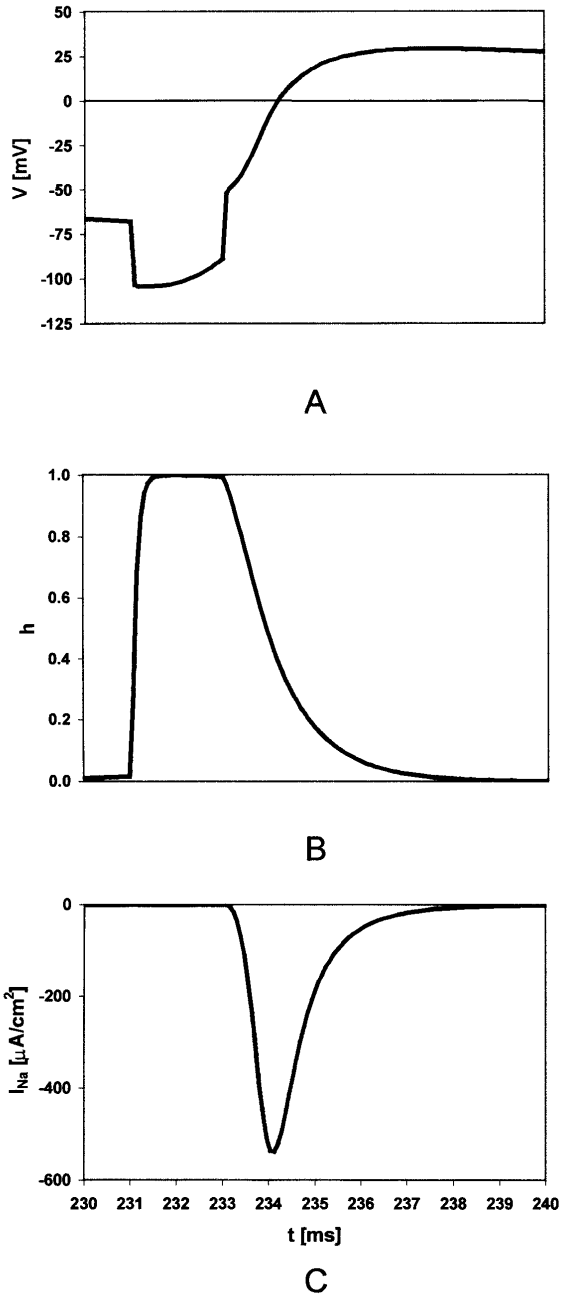

Figure 7. Anodal effect of a premature stimulus. Same pulse arrangement as in Fig. 6 except for the duration of the premature pulse (2 rather than 0.5 ms). Records refer to the right end of cell 4 ($x = 0.08$ cm). **A.** Time course of membrane potential; **B.** changes in availability of the Na system; **C.** development of Na current after stimulus break.

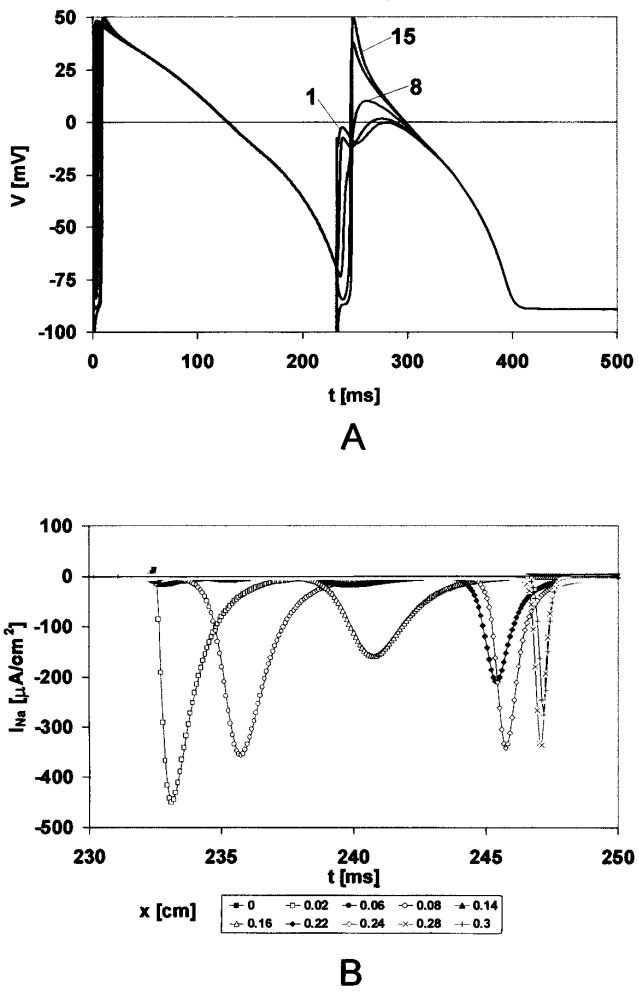

Figure 8. Stimulation at $t_2 = 232$ ms. **A.** Voltage responses on a large time scale. Traces are classified by the cell numbers and refer to the right end of a cell. **B.** Na currents following the premature stimulus. Sites of records are distinguished by different symbols.

2. Graded nature of refractory phenomena

The refractory behavior of a fiber changes markedly when J_2 and R_j are varied over a wide range. The larger the values of J_2 and R_j, the more pronounced is the immediate stimulus effect, namely, the local de- and hyperpolarizations induced at the ends of a cell. This in turn affects the current and voltage responses which develop after the break of the stimulus.

The effect of increasing J_2 (at a given level of R_j) is as follows. As shown above three types of responses (action potential prolongation, decremental conduction, or a new action potential) are observed when a rather weak stimulus is applied at various times. The main effect of increasing J_2 is that the interphase, characterized by decremental voltage responses, gets progressively shortened. This implies a shortening of the refractory period. When the stimulus strength reaches a critical value ($\hat{J}_2$), the interphase shrinks to zero duration, that is, decremental conduction is no longer seen with stimuli above $\hat{J}_2$. Under these conditions a simple definition of the refractory period is difficult. Actually what we observe with increasing delay of the premature stimulus is a continuous transition from a prolongation of the basic action potential to the generation of a new action potential, both types of response being nondecremental in nature. Like the voltage responses, the current patterns fail to show abrupt changes when the stimulus delay is varied.

Generally, the value of $|\hat{J}_2|$ decreases with increasing R_j. For the standard value, $R_j = 0.33$ MΩ, $\hat{J}_2$ is around -75 mA/cm^2 (which is about 8-times the diastolic threshold current). For $R_j = 1, 3, 10$ MΩ, $\hat{J}_2$ comes to -45, -35 or -25 mA/cm^2, respectively. Thus, the range of stimulus strength that allows a clear definition of the refractory period is more and more restricted with increasing junctional resistance.

3. Conduction velocity as function of R_j and J_2

Like a normal action potential, propagation of an extrasystole is progressively accelerated when stronger stimuli and/or higher R_j are accounted for (Section A). Acceleration of signal conduction is primarily related to the interior cells of a fiber. As an extreme case, an approximate synchronization of electrical activity may be reached. An example for this effect is given in Fig. 9.

4. Long vs. short fibers

The simulations described so far all refer to short chains of 15 cells (fiber length 0.3 cm). In longer fibers the refractory phenomena are in principle the same but the time dependence is shifted. This is mainly due to a slight prolongation of the conditioning action potential, namely, a delay of final repolarization in longer fibers. For a 100 cell fiber (length 2 cm), the delay is of the order of some ms relative to a short fiber and a similar delay is seen with the different refractory phenomena. Thus, the refractory period is extended by few ms in a fiber of 100 cells. For even longer fibers, no further delay in recovery was observed.

In Table 2, the data obtained from long fibers are summarized. At a given value of R_j, the refractory period is progressively shortened with increasing J_2. This corresponds to the normal configuration of a strength-interval diagram. For a given stimulus stronger than 16 mA/cm^2 the duration of the refractory period decreases with increasing R_j. For weaker stimuli, approaching the diastolic threshold value, that relation is not valid.

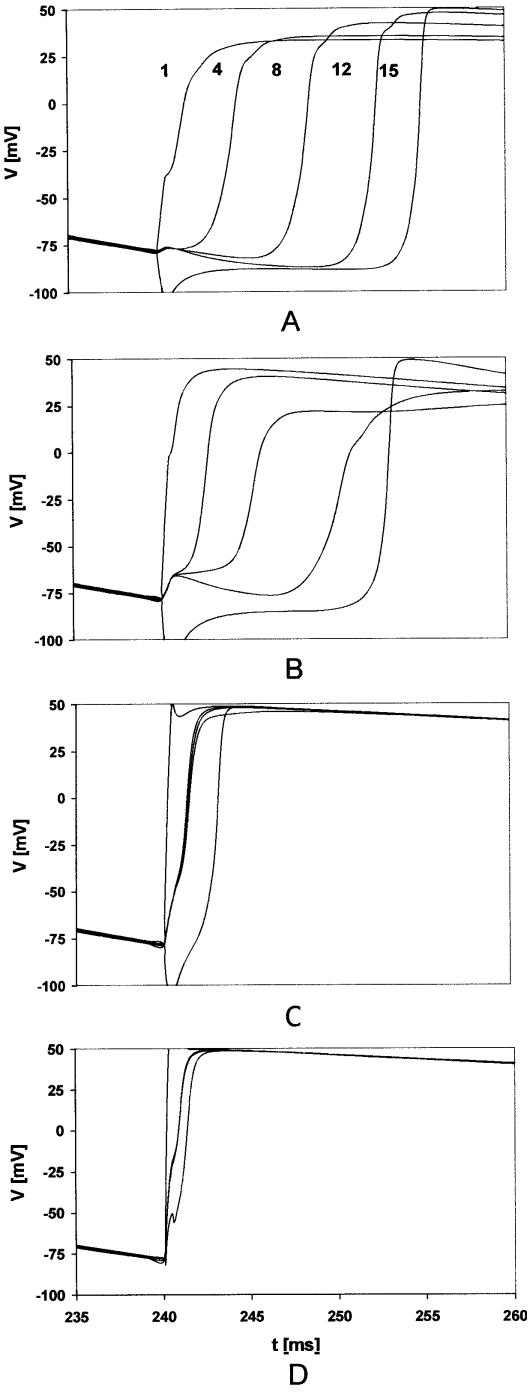

Figure 9. Conduction velocity of an extrasystole as a function of stimulus strength (J_2). Measurements refer to a 15 cell fiber with $R_j = 3$ MΩ. Premature stimuli were applied at $t_2 = 240$ ms. Shown is the rising phase of the signal in cells 1, 4, 8, 12, and 15 (center of a cell), using stimuli of -25, -50, -100, and -150 mA/cm^2 (A–D).

Table 2. Influence of disk resistance (R_j) and stimulus strength (J_2) on the duration of the refractory period (RP)

R_j (MΩ)	0.33	1	3
J_2(mA/cm^2)	RP (ms)		
−10	246		
−12	244	245	
−14	243	243.4	244
−16	242.7	242	240
−18	242.5	241	238
−20	242.3	239.5	237.5
−25	242	237.8	236
−30	241	237.3	235
−40	239.8	237	
−50	239		
−60	238		

Data refer to fibers consisting of 100 cells (fiber length 2 cm). The conditioning action potential was initiated by a current pulse (−25 mA/cm^2; 0.5 ms) applied at zero time. Test pulses between −10 and −60 mA/cm^2 were used to determine the functional refractory period. All data were derived from simulations where generation of an extrasystole was clearly distinguishable from decremental waves elicited at shorter stimulation intervals, using stimuli $|J_2| < |\hat{J}_2|$.

Section C. Disk resistance and vulnerability

It is generally agreed that the naturally existing nonuniform recovery of excitability is of major importance for the genesis of reentrant arrhythmias in cardiac tissue and a single induction shock, impinging on cells that are just coming out of their refractory period, can initiate flutter or fibrillation. In Section B it was shown that fibers differing in junctional resistance also differ in the duration of the refractory period. Thus, it is conceivable that inhomogeneities in R_j may give rise to unidirectional block and reentry in response to a properly timed premature stimulus.

To demonstrate this effect, we use the ring-shaped model depicted in Fig. 1B, with the specification that the two branches of ring are assigned different values of R_j, namely, $R_j = 0.33$ MΩ in the right branch (representing the normal permeability of intercellular contact in cardiac muscle) and $R_j = 1$ MΩ in the left branch. Circumference of ring is taken as 8 cm which should be long enough for a short signal travelling with relatively low speed. A brief current pulse J applied between anode (bottom) and cathode (top of ring) will flow as $\sim J/2$ through either branch because the extracellular pathways of the two branches are identical.

1. Generation of circus movement

Fig. 10 illustrates the effect of a two-pulse stimulation, using current pulses of equal (rather low) intensity (50 mA/cm^2, which is equivalent to about 25 mA/cm^2 for

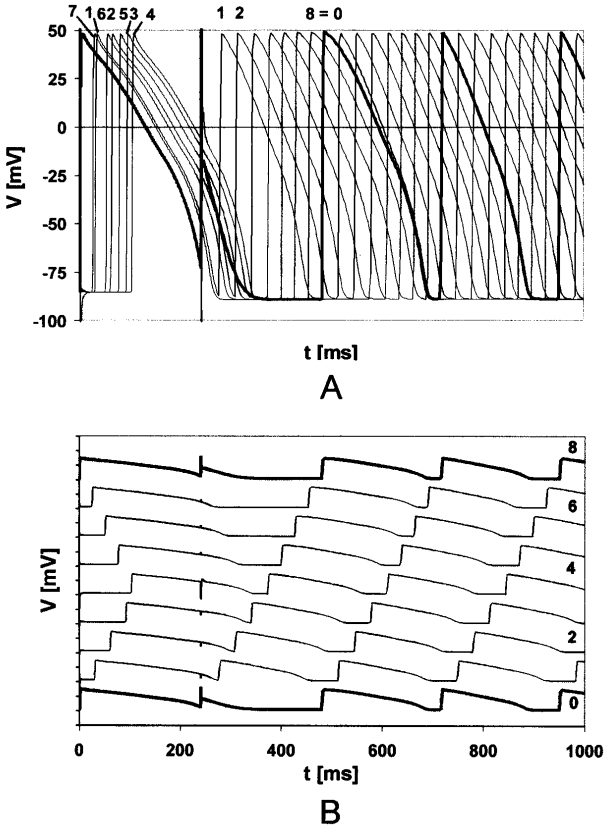

Figure 10. Sustained reentry of a premature action potential in a one-dimensional ring structure (400 cells of 0.02 cm in length; Fig. 1B). Bipolar external stimulation between $x = 0$ (cathode) and $x = 4$ cm (anode). R_j is set to 1 MΩ in the left branch of ring ($0 < x < 4$ cm) and 0.33 MΩ in the right branch ($4 < x < 8$ cm). Shown are the voltage responses of cells $50, 100 \ldots 400$ (corresponding to $x = 1, 2 \ldots 8$ cm) elicited by two current pulses ($J_1 = J_2 = -50$ mA/cm^2; 0.5 ms) applied at an interval of 240 ms. **A.** Superposition of voltage traces in a uniform time-voltage diagram. Propagation of the extrasystole is in counterclockwise direction. Thick lines represent the signal at the top of ring ($x = 0$). **B.** Separation of voltage traces by vertical displacement; vertical scale on the left edge of the diagram in steps of 100 mV. Numbers against the curves indicate the respective localization (in cm).

either branch). The first pulse initiates a full action potential which propagates from the cathode down the branches of ring so we have two wavefronts running in opposite directions and colliding at a site near the anode. Due to the difference in R_j, the wave in the left branch is expected to exhibit a shorter refractory period than the wave does in the right branch. According to the data listed in Table 2,

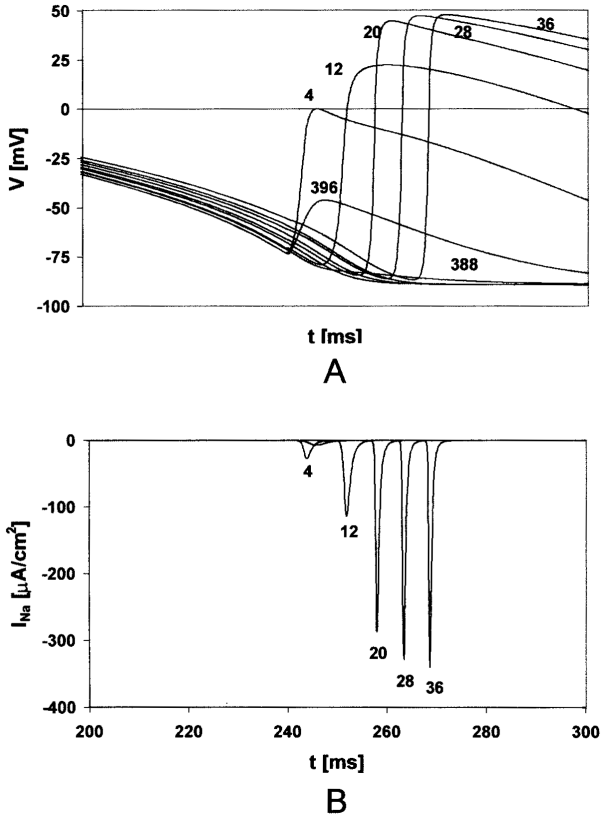

Figure 11. Development of unidirectional block in the two-pulse experiment shown in Fig. 10. Membrane responses to the premature stimulus are presented on an expanded time scale. **A.** Transmembrane voltage; **B.** Na currents of different cells located near the cathode (recorded from the center of a cell). Numbers against the curves indicate the sequence of cells.

the respective values (related to an extrastimulus of 25 mA/cm^2) are 237.8 and 242 ms. Thus, when the second pulse is applied at a time between these values, namely, 240 ms, a new action potential is generated in the left branch while the right branch merely exhibits passive distortions of the basic action potential. The new action potential has the full height of a regenerative signal and a duration of about 225 ms. It passes the collision point of the conditioning action potentials and travels through the full circle in multiple repetitions with a speed of about 34 cm/s. Thus, the wavelength of the circulating impulse (the product of conduction velocity and signal duration) tightly fits the length of the circular pathway (see the "leading circle concept" demonstrated by Allessie et al. 1973, 1976, 1977; Smeets et al. 1986).

Fig. 11 illustrates the initiation of circus movement in more detail. At the time of premature stimulation, the conditioning action potential has repolarized to a level of about −73 mV at the cathode and the availability of the Na system is no more than about 5 %. However, this is sufficient for the development of a regenerative signal in the left branch. This is clearly seen from the behavior of excitatory Na current (Fig. 11B). While this current is very small in cell 4, it steeply increases with increasing distance from the cathode and approaches a value which is comparable to the Na current underlying the upstroke of a normal action potential. Correspondingly, amplitude and rising velocity of the signal grow up into the normal range (Fig. 11A). In contrast to the left branch, the right one is unable to produce a regenerative response. Na currents are practically zero and the voltage deflections due to the premature impulse fade away with increasing distance from the cathode. This is the basis of unidirectional block.

As expected, there is a time window ("vulnerable window", VW_{time}) for induction of reentry. To determine the window, we varied the time of premature stimulation, starting from $t_2 = 240$ ms, in steps of ± 0.2 ms. This procedure resulted in a window reaching from 238.6 to 241.6 ms which roughly corresponds to the different refractory periods of the two branches. Fig. 12 illustrates what happens when the premature stimulus is timed outside the window. At $t_2 = 238$ ms, the effect appears as a prolongation of the conditioning action potential in either branch of ring; at $t_2 = 242$ ms, the response is an extrasystole in both branches. In either case, there are two opposing waves of excitation which extinguish one another by collision.

We further investigated the effect of an increased stimulus strength on generation of circus movement. When the stimulus was doubled ($J_2 = -100$ mA/cm^2), the window reached from 239.2 to 248 ms, i.e., the width of VW_{time} was markedly increased. With even stronger stimuli, the opposite effect was seen: the window became narrower and shrank to zero duration with stimuli around 200 mA/cm^2, i.e., if J_2 exceeds a certain level reentry will not occur no matter what the moment of stimulation is. Thus, the model exhibits an "upper limit of vulnerability" similar to that observed in animal studies (Chen et al. 1986). In our model, the upper limit is around 200 mA/cm^2, corresponding to a longitudinal field strength of about 18 V/cm.

A qualitative explanation for this behavior may be obtained from the results described in Section B(2.), considering the two branches of ring as separate fibers exposed to half the stimulating current.

Two complications are met when premature stimulus strength is increased. First, a clear definition of the refractory period is lost when the stimulus strength exceeds a critical value. This is mainly due to the occurrence of multiple Na currents induced by polarization of the individual cells. The critical value of stimulus strength depends on the junctional resistance of a fiber and decreases with increasing R_j. For a stimulus current $J_2 = -100$ mA/cm^2 applied to the ring as a whole, $J_2/2$ is below the critical value in the right branch but above the critical value in the left branch. Thus, the refractory period is well defined on the right side

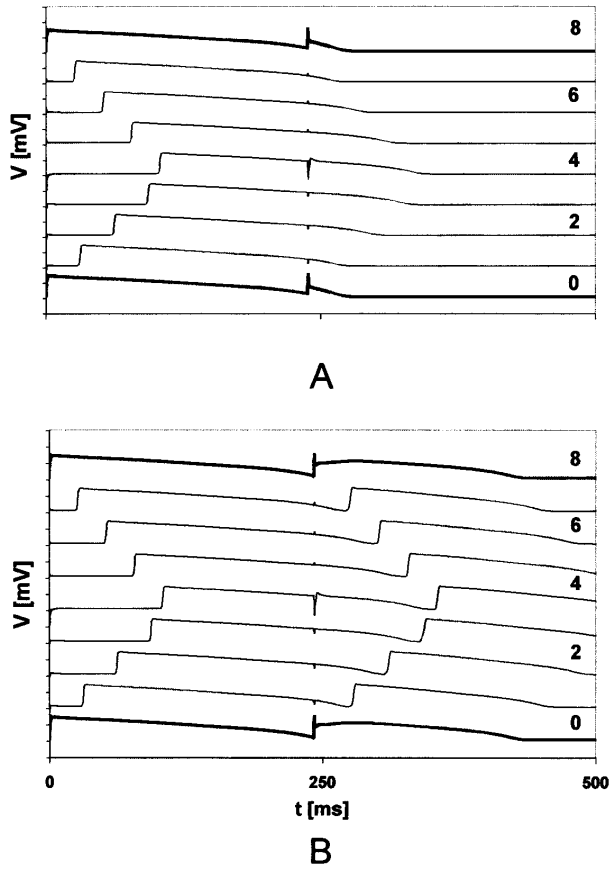

Figure 12. Definition of the vulnerable window. Voltage responses of the ring-shaped model with a stimulus delay of 238 (A) and 242 ms (B). Arrangement of the records as in Fig. 10B.

(239 ms) but cannot be predicted for the left side. Actually, the effect is as if the refractory period of the left branch (with the higher R_j) were *longer* than that in the right branch – just opposite to the case $J_2 = -50$ mA/cm^2. This is manifested by a reversion of the circulating wave which now runs clockwise rather than counterclockwise (not shown). Thus, the upper end of VW_{time} seems to reflect the refractory period of the left branch. For a stimulating current $J_2 = -150$ mA/cm^2, the stimulus is above the critical value in either branch and multiple Na currents occur all over the ring. There is no essential difference in the reaction of the two branches which means a decreased proneness to reentry.

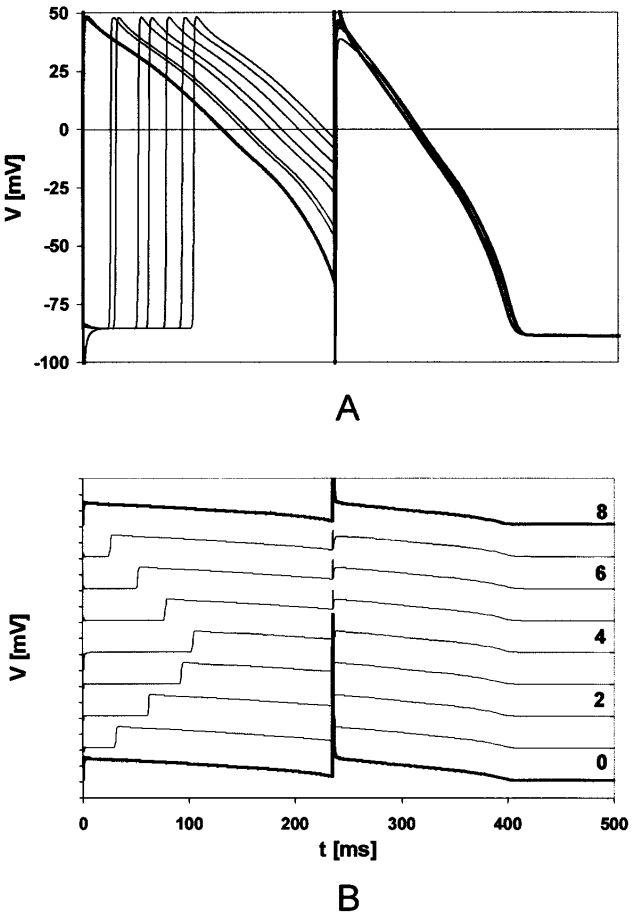

Figure 13. Synchronization of voltage responses associated with a strong premature stimulus ($J_2 = -300$ mA/cm^2; $t_2 = 235$ ms). The conditioning action potential was initiated by a current pulse of -50 mA/cm^2. Arrangement of the records as in Fig. 10. For further explanation see text.

The second complication is that the propagation velocity of an extrasystole increases with increasing stimulus strength (Fig. 9), tending to a "synchronization" of the excitation process over most of the fiber. This effect is clearly seen in Fig. 13. When a current pulse of 300 mA/cm^2 is applied, the reaction of the ring is very simple: the cells are all activated at the same time and produce a signal of uniform size and duration which may be referred to as a "synchronized extrasystole". Obviously, such a signal cannot result in a circus movement because an excitable gap is missing.

As to the mechanism underlying a synchronized extrasystole, the essential point is where the excitatory Na currents come from. Again the "sawtooth effect" seems to be basic for the generation of those currents. At t_2, different cells of the ring are in different states of refractoriness, depending on the degree of repolarization of the conditioning action potential. A strong stimulus causes a strong polarization of the individual cells: depolarization at the cathodal end and hyperpolarization at the other end. Cells which are in a recovered state produce Na currents in response to depolarization; cells which are in the refractory state may generate Na currents in response to anodal break. In this view, most cells are capable to produce excitatory Na currents no matter what the moment of premature stimulation is. This is the basis for the uniform reaction of the ring.

2. Suppression of circus movement

The nonuniform ring model used in this study does not only imply initiation of reentry but also termination of unidirectional propagation by a "defibrillatory" shock.

This effect is demonstrated in Fig. 14. The self-sustained travelling wave is the same as in Fig. 10. Circus movement is stopped when a current pulse of 250 mA/cm^2 (which is about 12-times the diastolic threshold) is applied during the second revolution. The time of current application is taken in an arbitrary manner. The shock results in a sudden, generalized depolarization of the ring fiber: each cell produces a signal resembling a short-lasting action potential and all cells are activated within a few ms after the shock. Repolarization of the signal leads to electrical arrest at the level of resting potential. Obviously, the synchronous nature of the shock-induced signal is not compatible with unidirectional propagation.

In Fig. 15, the shock intensity is increased to 350 mA/cm^2. Again the effect is a prompt cessation of circus movement. The terminating signal appears as an extrasystole which is almost perfectly synchronized all over the ring (Fig. 15A,B). This may be understood as an extreme consequence of the sawtooth effect, that is, the local de- and hyperpolarizations induced by the shock. At the time of shock application ($t_3 = 670$ ms) the state of refractoriness will be different in different cells, depending on the actual membrane potential. In the case of Fig. 15, the majority of cells – namely, all cells between $x = 1$ cm and $x = 6$ cm, i.e., 250 of a total of 400 cells – are in a state of absolute refractoriness because the respective membrane potentials prior to the shock are between -62 mV ($x = 1$ cm) and 45 mV ($x = 6$ cm) so that the availability of the Na system is almost zero. These cells are unable to produce a Na current in response to local depolarization. However, the local hyperpolarizations may result in strong Na currents of the anode break type.

This effect is illustrated in Fig. 15C. The cells 50, 100, and 150 ($x = 1, 2, 3$ cm) are representative of the left branch of ring ($R_j = 1$ MΩ). The membrane potential just prior to the shock is -62 mV in cell 50 and -6 mV in cell 150. At the break of the shock ($t = 670.5$ ms) the cells are hyperpolarized to -190 and -167 mV, respectively, at their anodal ends (not shown) and strong Na currents

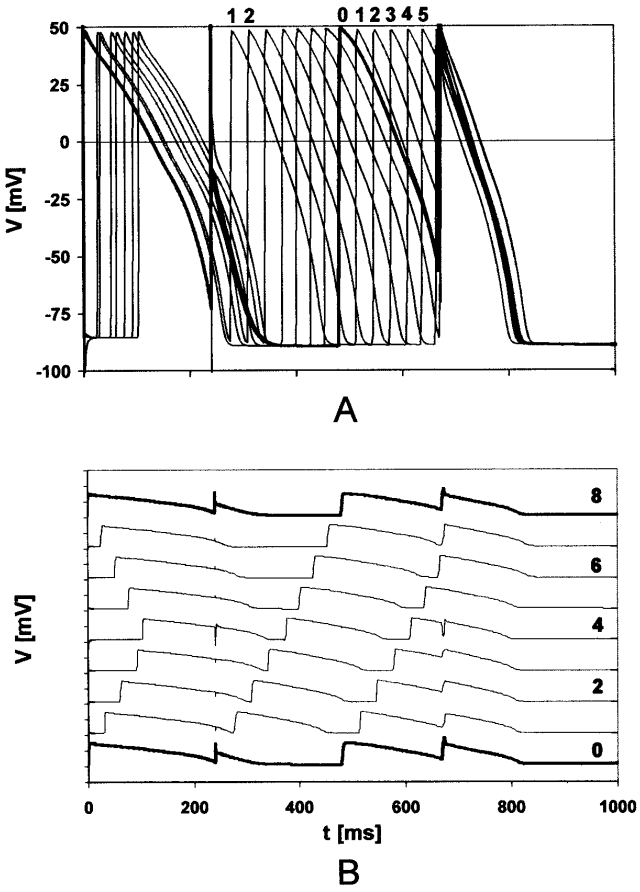

Figure 14. Suppression of reentry by electrical shock. Ring fiber of 400 cells with nonuniform distribution of junctional resistance (Fig. 10). Three current pulses were delivered through the same electrode arrangement. The first two pulses ($J_1 = J_2 = -50$ mA/cm^2; $t_2 = 240$ ms) were used to initiate a circus movement. A strong current $J_3 = -250$ mA/cm^2 (0.5 ms in duration) applied at $t_3 = 670$ ms causes an abrupt termination of the circulating wave. Voltage traces are shown in superposition (A) and in separate arrangement (B). Numbers against the curves indicate location in cm.

develop within half a ms. Cell 200 represents the transition from the left to the right branch and produces a Na current with a delay of about 1 ms.

In the right branch of ring the junctional resistance is lower ($R_j = 0.33$ MΩ) and the polarizing effect of the shock is less pronounced. Cells 250 and 300 are in an early phase of repolarization (37 and 45 mV, respectively) at shock incidence and undergo a hyperpolarization to −68 and −57 mV at their anodal ends. Under

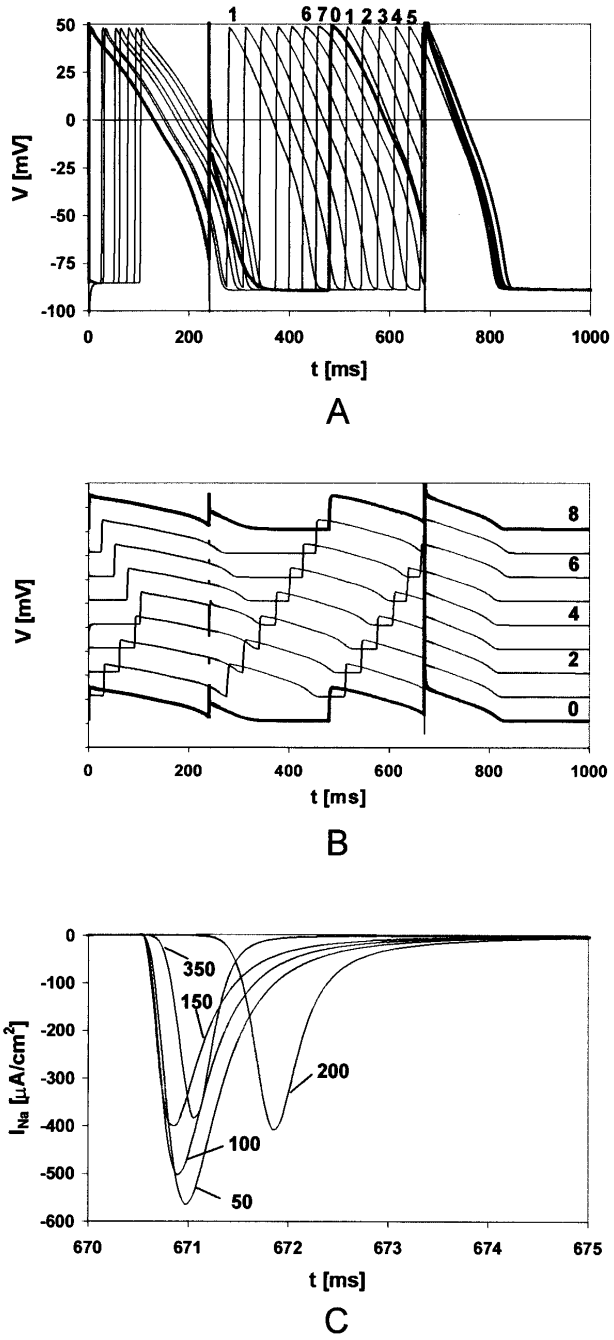

Figure 15. Voltage and current responses to a "defibrillatory" shock of 350 mA/cm^2 applied at t_3 = 670 ms. **A.**, **B.** Voltage traces on a macroscopic time scale; arrangement as in Fig. 14. **C.** Na currents induced by the shock in different cells of ring fiber. Numbers against the curves indicate the cell sequence. Currents are all recorded from the anodal end of a cell and are shown on an expanded time scale. Note that distance (x) and cell number (N) are taken in a counterclockwise direction, with the origin at the cathode (top of ring) so that cells 50 and 350 are in a symmetrical location with respect to the cathode.

these conditions an anode break effect is not possible. Those cells are "silent" in a sense that they do not produce Na currents at all, neither in the depolarized half of a cell nor in the hyperpolarized half. Quite different is the reaction of cell 350. This cell is almost fully repolarized (−84 mV) prior to the shock and produces a Na current at the depolarized end (not shown) as well as at the hyperpolarized end.

The above example suggests that structural discontinuities of heart muscle (represented by intercalated disks) may play an important role in the process of "defibrillation" under real conditions. A strong sawtooth effect could act as link between the externally applied shock and the reaction of the cells. Excitatory Na currents may occur in large regions of cardiac tissue, no matter whether the cells are in an excitable or in a refractory state. The result is a synchronized activation and inactivation of the tissue which may be considered as the basic mechanism for an extinction of circulating wavefronts.

An interesting finding in our simulations is that the upper limit of vulnerability is close to the minimum current strength required for suppression of circus movement (about 200 and 220 mA/cm^2, respectively). In other words, a stimulus that is too strong to initiate unidirectional propagation is just sufficient to suppress a reentrant wave elicited by a weaker stimulus. This is in accordance with experimental observations on open-chest dogs (Chen et al. 1986). The near coincidence of the two limiting values suggests that they are based on a similar mechanism. This is actually the case in our model.

Discussion

1. The sawtooth effect – experimental vs. theoretical results

In a naïve view, the sawtooth effect seems a simple consequence of recurrent discontinuities of internal resistance in cardiac tissue. However, experimental evidence for a voltage jump at an intercellular junction during field stimulation is a controversial matter. The very essence of the sawtooth hypothesis lies in the fact that it could give a simple explanation for a "far-field" stimulation of cardiac tissue as is required for defibrillation. It is mainly for this reason that a number of experimental studies were performed in order to obtain direct evidence in favor of, or against, the sawtooth mechanism (for review see Roth 2001).

So far, a positive result has been obtained only with the simplest coupled system, namely, an isolated cell-pair (Sharma and Tung 2001). However, it is not clear whether the sawtooth effect is preserved in multicellular structures. Gillis et al. (2000) used a high-spatial-resolution optical mapping to record the field responses from cell monolayers of neonatal myocytes but failed to observe an abrupt change in polarity across the intercellular junctions. Zhou et al. (1998) used a double-barrel microelectrode technique to record field responses from guinea-pig papillary muscle. With a distance of 20 μm between the recording sites they were unable to detect a sawtooth pattern in the individual cells. The authors concluded that the

model of the sawtooth pattern is incorrect or that each sawtooth oscillation occurs over a bundle of cells instead of over a single cell.

In summary, the sawtooth effect is a hypothesis which could be of great interest for an understanding of cardiac dynamics but lacks a general verification by experimental data. However the fact that a hypothesis is hard to test does not imply that it is wrong. Thus, it seems reasonable to elaborate the theoretical aspects of the sawtooth effect in more detail in the hope to reconcile the theoretical with the experimental data.

2. Characterization of the model

The model used in this study was chosen to represent an excised cardiac fiber embedded in a confined volume of interstitial fluid. Gap junctions are understood as purely resistive elements and are lumped into the resistance of an intercalated disk (R_j). The disks are treated as discrete discontinuities of internal resistance. In planning the study, we were motivated by actual problems of electropathology, namely, induction and suppression of fibrillation by a current passed through the heart. To simulate this condition, we used an external current flow field for stimulation of a fiber. This mode of stimulation is different from that used in previous one-dimensional model studies (Rudy and Quan 1987, 1991; Quan and Rudy 1990; Shaw and Rudy 1995) which were based on intracellular current injection (point stimulation). The difference is important because the basic effect of external field stimulation, namely, a periodic oscillation of transmembrane potential reflecting the cellular structure of a fiber, is rudimentary in the case of an intracellular source (Krassowska et al. 1987). We found that potential jumps at the cell junctions develop very rapidly compared to the polarization of a continuous fiber so that a full effect is reached even with very brief current pulses (Krassowska et al. 1990).

3. The impact of sawtooth effect on refractoriness

The main concern of this study was a search for a possible interaction of intercalated disks with the refractory behavior of a fiber. To our knowledge, this problem has not been treated extensively in the literature. Systematic variations of junctional resistance (R_j), premature stimulus strength (J_2), and the time of stimulus application (t_2) yielded different types of responses. With low values of R_j and J_2, a prolongation of the conditioning action potential, a signal with decremental conduction, or a new action potential were observed when the premature stimulus was applied with increasing delay. In this case, the functional refractory period was clearly defined by an abrupt change from decremental conduction to a regenerative signal propagating without decrement. Unusual responses were observed with higher values of R_j or J_2: the phase of decremental conduction was shortened and finally disappeared so that only two types of responses remained, namely, action potential prolongation or generation of a new signal. Under these conditions, a simple definition of the refractory period was no longer possible. The diversity of responses has to do with the complex nature of Na current generation in a discontinuous fiber. The essential point is a sawtooth effect of the premature stimulus

resulting in multiple polarizations at the cell junctions so that Na currents may arise immediately in the individual cells. These currents are basic to a shortening of the refractory period observed with a (moderate) increase in R_j at a given J_2 (Table 2).

It is interesting to compare our simulations with experimental data obtained under conditions of field stimulation. There are numerous findings suggesting that the effect of a transcardiac shock much depends on the local shock intensity in the myocardium. The "critical point hypothesis" (Winfree 1983; Frazier et al. 1989) says that a rotor of reentry originates from a region where the shock field is relatively weak and then propagates into the region of a stronger field. This idea implies that the impact of a strong field cannot simply be explained by the classical concept of refractoriness. This problem has been extensively studied by Knisley et al. (1992) in experiments on rabbit papillary muscle. In this study, an external field was applied at various times of a conditioning action potential and the cellular response was recorded by intracellular microelectrodes. An effect of field strength on the voltage responses was clearly seen (Fig. 2 of that paper): with a weak field there was an abrupt change from a small unspecific response to the generation of a new action potential, allowing a clear definition of the refractory period. With increasing field strength the all-or-none effect was lost and was replaced by a gradual transition from prolongation of the basic action potential to initiation of a new signal so that the end of the refractory period was not clearly defined. The ionic mechanism of this effect remained unknown. In principle, the refractory phenomena observed by Knisley et al. (1992) are the same as those predicted by our model.

A further finding in Knisley's study was that an increase in field strength decreased the dispersion of repolarization (the variation of times of repolarization) following the shock. With strong fields (>10 V/cm) there was a time window during which dispersion was negligibly small, i.e., duration of the shock-induced signals was nearly constant regardless of the instant of field application (Fig. 5 of that paper). Transferred to the space domain, this observation means a tendency to a synchronization of the signals along the fiber. This is similar to the effect shown in Fig. 9 of the present study.

4. Unidirectional block and reentry

It is widely accepted that a spatial asymmetry in refractoriness is a determinant of vulnerability. Such an asymmetry may arise in two ways: either it is intrinsic, i.e., due to a nonuniformity of membrane or cable properties, or it is functional in nature, that is, the asymmetry results from local differences in recovery associated with the propagation of a normal action potential in an otherwise uniform structure.

The ring-shaped model used in this study is based on an intrinsic asymmetry in refractoriness resulting from an inhomogeneities in junctional resistance (R_j). To keep the model as simple as possible we considered the case of a step change in R_j between the two halves of ring so that an asymmetry of refractoriness was expected at the boundaries of the two branches. Stimulus current was applied by a pair of extracellular electrodes located at the boundaries of the two segments. The ring

model exhibits a circus movement when a premature stimulus (J_2) of appropriate strength is applied within a window reflecting the difference in refractory period duration. With increasing J_2, the vulnerable window, VW_{time}, first increases in width and then shrinks and an upper limit of vulnerability is reached with stimuli of ∼10-times the diastolic threshold. This behavior is explained by multiple Na currents arising from a strong sawtooth effect. For stimuli exceeding the upper limit of vulnerability the result is a nearly uniform signal with the characteristics of a "synchronized extrasystole".

A comparison with previous theoretical studies on reentry (Quan and Rudy 1990; Shaw and Rudy 1995) is difficult because of principal differences in the basic assumptions. The authors investigated vulnerability in a uniform one-dimensional ring of cardiac fiber and simulations were based on a "functional inhomogeneity" in refractoriness created by the conditioning action potential. Under these conditions, the tail of the conditioning wave includes a small segment (window) with a critical gradient of recovery. A premature stimulus which strikes the window may generate a new signal which propagates in the retrograde direction (the more recovered region) but fails to do so in the antegrade direction (the less recovered region). In the simulations, point sources (rather than field stimulation) were used for both the primary and the premature stimulus. These studies were mainly concerned with an influence of membrane Na conductance ($\overline{g_{\text{Na}}}$) and gap junctional resistance (R_j) on the genesis of a unidirectional block. In a few simulations (Quan and Rudy 1990; Fig. 6) the influence of premature stimulus strength on vulnerability was tested. The vulnerable window was found to monotonically increase with increasing stimulus strength and there was no indication of an upper limit of vulnerability. This is in contrast to our results and may be explained by the basic difference between point stimulation (as used by those authors) and field stimulation (used in the present study), namely, a strong sawtooth effect during field stimulation and a weak effect in the case of point stimulation.

5. The upper limit of vulnerability

It is well-known that a stimulus not only can be too weak to induce reentry but also can be too strong. That is, there exists a lower limit (fibrillation threshold) and an upper limit of vulnerability. Stimuli stronger than the upper limit may damage the heart in different ways, e.g. by heat development or by electroporation but they are unlikely to cause fibrillation. This is consistent with statistical data of electrical accidents showing that high-voltage injuries are usually not accompanied by ventricular fibrillation (D. Kieback, personal communication).

An upper limit of vulnerability is an inherent feature of the critical point hypothesis mentioned above. The hypothesis implies (in a two-dimensional context) that there exists a critical value of field strength determining the development of a unidirectional block when the tissue is exposed to an inhomogeneous electric field. Assuming a vertical configuration between "isorecovery lines" of a preceding action potential and "isogradient lines" of the applied field, the critical point is defined as intersection between the isorecovery line representing the end of the refractory

period and the isogradient line representing the critical field strength (Frazier et al. 1989, Fig. 4 and 11; Knisley et al. 1992). By mapping studies it was shown that a new activation wave started from a region where the field strength was lower than the critical strength while a temporary unidirectional block was generated in the region where the field was stronger than the critical value. This may give rise to a circus movement around the critical point. According to this hypothesis, a circulating wave cannot develop if the field is stronger than the critical value throughout the tissue.

Obviously, this interpretation does not hold for our one-dimensional model because the field pattern is quite different. In our ring model, the extracellular field associated with the premature stimulus is parallel to the wave of the primary action potential and the field is almost homogeneous in the two branches of ring. A stimulus of sufficient strength produces excitatory Na currents throughout the ring as a consequence of a strong sawtooth effect. The result is a uniform activation of the cells which appears as a synchronized extrasystole. Such a uniform activation does not allow reentry because the wavefronts will have nowhere to go. This is our explanation for an upper limit of vulnerability.

6. Termination of reentry

By clinical experience, ventricular fibrillation can be stopped by discharging a high-voltage electric pulse through the heart. At present, application of defibrillating shocks is a routine procedure for the treatment of life-threatening arrhythmias. In spite of its widespread use, the mechanism by which defibrillation is achieved is not fully understood. Different hypotheses have been developed to describe the requirements for a successful defibrillation but they do not really explain what happens at a cellular level.

A shock delivered *via* transthoracic electrodes generates an electric current field which may be of different size and direction in different regions of the heart. The shock current is not constrained to the extracellular fluid but passes into the intracellular pathway as well. In principle, the shock has a polarizing effect on the tissue, causing a hyperpolarization of the cell membrane at sites where current enters a cell and causing a depolarization where current leaves the intracellular space. De- and hyperpolarization are inevitably interconnected. The question, then, is what the pattern of polarization looks like and which reactions develop from de- and hyperpolarized sites. In general, the response of a cell will depend on its electric state just prior to the shock and the transmembrane potential changes induced by the shock. This is, of course, an abstract formulation which may be given a concrete meaning only by use of particular assumptions.

In our simulations using a ring-shaped model of a discontinuous fiber, a "defibrillating" effect is easy to be demonstrated. Circus movement is promptly terminated when a strong current pulse (J_3) is passed through the ring (Figs. 14, 15). The basic mechanism is a polarization of the individual cells at the cell junctions (sawtooth effect). As a second step excitatory Na currents occur in the bulk of tissue, either due to depolarization of the cathodal end of a cell (when the cell was

in a recovered state) or due to a release of hyperpolarization at the anodal end (when the cell was in a refractory state). This results in an overall activation which is manifested as a synchronized extrasystole throughout the ring. This is equivalent to a termination of reentry.

In this interpretation the sawtooth effect is the main element of defibrillation. The question, then, is whether this concept goes together with experimental data of defibrillation research. Electrophysiological studies of the effect of a defibrillating shock *in vivo* or *in vitro* are complicated by strong artifacts associated with shock current flow. A direct measurement of the voltage responses by use of conventional microelectrodes is limited by large voltage gradients produced by the shock. It is for this reason that earlier studies were mainly related to effects observed after, rather than during, shock application (Knisley et al. 1992; Jones and Jones 1982; Sweeney et al. 1991). The main finding was a general increment in refractoriness in the shock-exposed tissue, either due to the repolarizing phase of directly excited cells or to a repolarization delay (prolongation of the depolarized state) in cells already undergoing an action potential. An essential progress was the introduction of optical methods using voltage-sensitive dyes (Dillon 1991; Knisley et al. 1993). Optical methods are free of artifacts caused by the shock current flow, thus allowing an uninterrupted voltage recording. However, optical methods are less specific than microelectrode recordings because they sense the activity of a population of cells rather than a single cell and an absolute voltage calibration is not possible.

In an extensive study on isolated rabbit hearts, the characteristics of the defibrillation process were analyzed (Dillon 1991, 1992). Fibrillation was induced by rapid pacing and defibrillation shocks were delivered through a pair of gross electrodes placed at the base and apex of the heart. Optical records from single sites of the epicardium were taken during several cycles of fibrillation preceding a defibrillation shock as well as during and after the shock. The important finding was that defibrillating shocks, applied at various times of the last fibrillation cycle, always caused a rapid depolarizing deflection followed by a slow phase of repolarization and that the repolarization time was constant, no matter whether the shock was applied during the plateau or during the final repolarization of the fibrillation action potential. Dillon (1992) described this as a "synchronized repolarization" and interpreted this effect as due to the generation of a new action potential by the shock. This looks strange for the case that the cells are in a refractory state (which is, because of the rapid sequence of fibrillation signals, the most likely state) at the moment of shock incidence and thus would be unable to produce excitatory Na currents in response to depolarization. As a hypothetical explanation, he proposed a hyperpolarizing effect of the shock on part of the cell membrane (Fig. 10 in Dillon 1991), leading to a recovery of the Na system and an activation of Na currents after the break of shock. However, this idea could not be quantified because hyperpolarizing effects of the shock were not seen in the optical voltage recordings and an identification of membrane currents was not possible.

Correlations between the data described above and the simulations presented in this paper are obvious. The synchronized repolarization as the typical shock effect

in Dillon's terminology is essentially equivalent to the synchronized extrasystole observed in our simulations (Figs. 14, 15). We prefer the latter term because it expresses the active nature of the signal more directly. The hyperpolarizing effect of a shock hypothesized by Dillon is an inherent feature of our model as a consequence of the sawtooth effect. In the bulk of cells excitatory Na currents are generated by an anode break effect so that this mechanism seems to be basic to a termination of circus movement. It should be noted that, under conditions of real fibrillation, the intracellular Ca^{2+} level is likely to increase because an augmented Ca^{2+} influx is not fully compensated by Ca^{2+} pumping mechanisms. An increase in internal Ca^{2+}, in turn, is known to increase the gap junction resistance (Maurer and Weingart 1987) so that a sawtooth effect would be accentuated under these conditions.

A further point of interest is the correlation between the upper limit of vulnerability and the defibrillation threshold. During fibrillation, wave fronts are thought to wander randomly throughout the tissue. A successful defibrillation does not only imply an extinction of circulating waves but also must prevent a generation of new waves which might lead to a resumption of fibrillation after the shock. Thus, the minimum stimulus strength required for defibrillation should be equal to, or greater than, the upper limit of vulnerability. This hypothesis was tested by Chen et al. (1986) in experiments on open-chest dogs using different electrode configurations. The authors found that the defibrillation threshold was not significantly different from, or slightly higher than, the upper limit of vulnerability. The same is seen in our simulations. Furthermore, our model explains how the coincidence of the two phenomena comes to pass. It is based on a common mechanism, namely, the occurrence of a synchronized extrasystole as the consequence of the sawtooth effect.

Conclusion

The simulations presented in this paper show that the junction resistance between neighbouring cardiac cells can have a distinct influence on the cells' responses to an applied extracellular electric field. The basic field effect is a polarization of the transmembrane potential of the individual cells (sawtooth effect) which, in turn, may affect the kinetics of membrane ionic currents. From the cellular polarization a number of effects may be deduced, e.g. a shortening of the refractory period by an increase in junctional resistance and an acceleration of signal propagation by increasing stimulus strength. Both effects are involved in the vulnerability phenomena. The upper limit of vulnerability is close to the defibrillation threshold and the determining voltage signal is a synchronized extrasystole in both cases. These data, obtained from a one-dimensional model of a cardiac fiber, suggest that the sawtooth mechanism, due to a periodic intercalated disk structure, could play a role in the defibrillation process in real myocardium.

Acknowledgements. The authors express sincere appreciation to the Professional Association for Precision Mechanics and Electrical Engineering Industries, Cologne, Germany,

for generous support for this work. The authors additionally wish to thank Juergen Dembski for preparing the computer graphics as well as Sabine Michels and Joydeep Mukherjee for their help in preparing the manuscript.

References

Allessie M. A., Bonke F. I. M., Schopman F. J. G. (1973): Circus movement in rabbit atrial muscle as a mechanism of tachycardia. Circ. Res. **33**, 54—62

Allessie M. A., Bonke F. I. M., Schopman F. J. G. (1976): Circus movement in rabbit atrial muscle as a mechanism of tachycardia. II. The role of nonuniform recovery of excitability in the occurrence of unidirectional block, as studied with multiple microelectrodes. Circ. Res. **39**, 168—177

Allessie M. A., Bonke F. I. M., Schopman F. J. G. (1977): Circus movement in rabbit atrial muscle as a mechanism of tachycardia. III. The "leading circle" concept: A new model of circus movement in cardiac tissue without the involvement of an anatomical obstacle. Circ. Res. **41**, 9—18

Antoni H. (1992): Definition and mechanism of refractoriness. In: Electrical Stimulation and Electropathology (Ed. J. P. Reilly), pp. 145—147, Cambridge University Press

Cartee L. A., Plonsey R. (1992): Active response of a one-dimensional cardiac model with gap junctions to extracellular stimulation. Med. Biol. Eng. Comput. **30**, 389—398

Chen P. S., Shibata N., Dixon E. G., Martin R. O., Ideker R. E. (1986): Comparison of the defibrillation threshold and the upper limit of ventricular vulnerability. Circulation **73**, 1022—1028

DiFrancesco D., Noble D. (1985): A model of cardiac electrical activity incorporating ionic pumps and concentration changes. Philos. Trans. R. Soc. London, Ser. B **307**, 353—398

Dillon S. M. (1991): Optical recordings in the rabbit heart show that defibrillation strength shocks prolong the duration of depolarization and the refractory period. Circ. Res. **69**, 842—856

Dillon S. M. (1992): Synchronized repolarization after defibrillation shocks. A possible component of the defibrillation process demonstrated by optical recordings in rabbit heart. Circulation **85**, 1865—1878

Frazier D. W., Wolf P. D., Wharton J. M., Tang A. S. L., Smith W. M., Ideker R. E. (1989): Stimulus-induced critical point: Mechanism for electrical initiation of reentry in normal canine myocardium. J. Clin. Invest. **83**, 1039—1052

Gillis A. M., Fast V. G., Rohr S., Klber A. G. (2000): Mechanism of ventricular defibrillation. The role of tissue geometry in the changes in transmembrane potential in patterned myocyte cultures. Circulation **101**, 2438—2445

Hodgkin A. L., Huxley A. F. (1952a): The dual effect of membrane potential on sodium conductance in the giant axon of Loligo. J. Physiol. (London) **116**, 497—506

Hodgkin A. L., Huxley A. F. (1952b): A quantitative description of membrane current and its application to conduction and excitation in nerve. J. Physiol. (London) **117**, 500—544

Hoffman B. F., Cranefield P. F. (1960): Electrophysiology of the heart. McGraw-Hill Book Co., New York, pp. 211—256

Jones J. L., Jones R. E. (1982): Determination of safety factor for defibrillator waveforms in cultured heart cells. Am. J. Physiol. **242**, H662—670

Knisley S. B., Smith W. M., Ideker R. E. (1992): Effect of field stimulation on cellular repolarization in rabbit myocardium. Circ. Res. **70**, 707—715

Knisley S. B., Blitchington T. F., Hill B. C., Grant A. O., Smith W. M., Pilkington T. C., Ideker R. E. (1993): Optical measurements of transmembrane potential changes during electric field stimulation of ventricular cells. Circ. Res. **72**, 255—270

Krassowska W., Pilkington T. C., Ideker R. E. (1987): Periodic conductivity as a mechanism for cardiac stimulation and defibrillation. IEEE Trans. Biomed. Eng. **34**, 555—560

Krassowska W., Pilkington T. C., Ideker R. E. (1990): Modeling excitation with extracellular electrodes. Pacing. Clin. Electrophysiol. **13**, 548

Krassowska W., Cabo C., Knisley S. B., Ideker R. E. (1992): Propagation versus delayed activation during field stimulation of cardiac muscle. Pacing. Clin. Electrophysiol. **15**, 197—210

Maurer P., Weingart R. (1987): Cell pairs isolated from guinea pig and rat hearts: effects of $[Ca^{2+}]_i$ on nexal membrane resistance. Pflgers Arch. **409**, 394—402

Plonsey R., Barr R. C. (1986a): Effect of microscopic and macroscopic discontinuities on the response of cardiac tissue to defibrillating (stimulating) currents. Med. Biol. Eng. Comput. **24**, 130—136

Plonsey R., Barr R. C. (1986b): Inclusion of junction elements in a linear cardiac model through secondary sources: application to defibrillation. Med. Biol. Eng. Comput. **24**, 137—144

Plonsey R., Barr R. C., Witkowski F. X. (1991): One-dimensional model of cardiac defibrillation. Med. Biol. Eng. Comput. **29**, 465—469

Quan W., Rudy Y. (1990): Unidirectional block and reentry of cardiac excitation: A model study. Circ. Res. **66**, 367—382

Roth B. J. (2001): Sawtooth effect: fact or fancy? J. Cardiovasc. Electrophysiol. **12**, 1174—1175

Rudy Y., Quan W. (1987): A model study of the effects of the discrete cellular structure on electrical propagation in cardiac tissue. Circ. Res. **61**, 815—823

Rudy Y., Quan W. (1991): Propagation delays across cardiac gap junctions and their reflection in extracellular potentials: A simulation study. J. Cardiovasc. Electrophysiol. **2**, 299—315

Sharma V., Tung L. (2001): Theoretical and experimental study of sawtooth effect in isolated cardiac cell-pairs. J. Cardiovasc. Electrophysiol. **12**, 1164—1173

Shaw R. M., Rudy Y. (1995): The vulnerable window for unidirectional block in cardiac tissue: Characterization and dependence on membrane excitability and intercellular coupling. J. Cardiovasc. Electrophysiol. **6**, 115—131

Smeets J. L. R., Allessie M. A., Lammers W. J. E., Bonke F. I. M., Hollen J. (1986): The wavelength of the cardiac impulse and reentrant arrhythmias in isolated rabbit atrium. The role of heart rate, autonomic transmitters, temperature, and potassium. Circ. Res. **58**, 96—108

Sweeney R. J., Gill R. M., Reid P. R. (1991): Characterization of refractory period extension by transcardiac shock. Circulation **83**, 2057—2066

Winfree A. T. (1983): Sudden cardiac death: A problem in topology. Sci. Am. **248**, 144—161

Zhou X., Knisley S. B., Smith W. M., Rollins D., Pollard A. E., Ideker R. E. (1998): Spatial changes in the transmembrane potential during extracellular electric stimulation. Circ. Res. **83**, 1003—1014

Appendix

A typical feature of the computer simulations presented in this paper is fluctuations in membrane potential within each cell, arising from external stimulus application. Thus, a sawtooth profile of membrane potential is generated reflecting the periodicity of junctional resistance along a discontinuous fiber. An unexpected finding was that polarization of the interior cells builds up much faster than is expected from the membrane time constant (Fig. 2). To get a better understanding of this phenomenon, a quantitative analysis of the polarizing effect would be useful.

The analytical approach is based on the following assumptions. A uniform fiber is subdivided into separate cells of length d by a periodic disk resistance. Active membrane properties are neglected. Thus, the electrical behavior of the fiber is determined by the parameters r_o, r_i, r_m, c_m, and R_j, with $\lambda^2 = r_m/(r_o + r_i)$ and $\tau_m = r_m c_m$ as derived quantities. Resting potential is set to zero level. The fiber is stimulated by a step current I applied at $t = 0$. The aim is to describe the membrane potential within an interior cell as function of distance and time. Within a cell, currents and potentials vary continuously and obey the classical cable equations. The basic assumption is that the voltage response of an interior cell is antisymmetric around the center of the cell and is identical with the voltage responses of the adjacent cells.

Taking the center of a cell as origin for the axial co-ordinate ξ, the cable equation for the transmembrane potential is

$$\lambda^2 \partial^2 V/\partial \xi^2 = V + \tau_m \partial V/\partial t \tag{4}$$

Because of the antisymmetry required it is sufficient to solve the equation for the interval $0 < \xi < d/2$. The boundary conditions, then, are

$$V = 0 \text{ for } \xi = 0 \text{ and } V = R_j i_i/2 = R_j(r_o I - \partial V/\partial \xi)/2(r_o + r_i) \quad \text{for } \xi = \mathrm{d}/2 \tag{5}$$

The solution may be obtained by use of the Laplace transformation. Denoting the Laplace transform of $(V\xi, t)$ by $U(\xi, s)$, the cable equation is replaced by the ODE

$$\lambda^2 \mathrm{d}^2 U/\mathrm{d}\xi^2 = U(1 + \tau_m s) \tag{6}$$

where s is the Laplace variable. The solution of equation (6) may be written as

$$U(\xi, s) = A \exp[-(\xi/\lambda)\sqrt{1 + \tau_m s}] + B \exp[(\xi/\lambda)\sqrt{1 + \tau_m s}] \tag{7}$$

where A and B are functions of s to be determined from the transformed boundary conditions

$$U = 0 \quad \text{for} \quad \xi = 0 \quad \text{and} \quad U = \frac{R_j}{2(r_o + r_i)}(r_o I/s - \mathrm{d}U/\mathrm{d}\xi) \quad \text{for} \quad \xi = d/2 \tag{8}$$

This yields the particular solution

$$U(\xi,s)=\frac{R_j r_\mathrm{o} I}{2(r_\mathrm{o}+r_i)s}\ \frac{\exp[-(\xi/\lambda)q]-\exp[(\xi/\lambda)q]}{(1-pq)\exp[-(d/2\lambda)q]-(1+pq)\exp[(d/2\lambda)q]} \tag{9}$$

where $p=R_j/2\lambda(r_\mathrm{o}+r_i)$ and $q=\sqrt{1+\tau_m s}$.

To obtain the original function $V(\xi,t)$ from the transform $U(\xi,s)$ we make use of the Bromwich integral

$$V(\xi,t)=\frac{1}{2\pi j}\oint U(\xi,s)\exp(ts)\mathrm{d}s \tag{10}$$

where the integral is taken over an appropriate contour in the complex s-plane, including the poles s_ν of $U(\xi,s)$.

The respective poles are the point $s_\mathrm{o}=0$ and the zeros of the right-hand denominator of equation (9). Zero condition for the denominator is

$$\exp[(d/\lambda)\sqrt{1+\tau_m s}]=(1-p\sqrt{1+\tau_m s})/(1+p\sqrt{1+\tau_m s}) \tag{11}$$

For this the root has to be a purely imaginary number, $\sqrt{1+\tau_m s}=bj$. Thus the zero condition is specified to

$$\begin{aligned}&\exp[j(bd/\lambda)]=(1-pbj)/(1+pbj)\ \ \text{or}\\&\exp\{j[bd/\lambda+2\ \operatorname{arctg}(pb)]\}=1\end{aligned} \tag{12}$$

which is equivalent to

$$bd/\lambda+2\ \operatorname{arctg}(pb)=2\pi\nu\ \ (\nu=1,2\ldots) \tag{13}$$

This goniometric equation may be solved by graphical or numerical methods, resulting in distinct values b_ν and poles $s_\nu=-(b_\nu^2+1)/\tau_m$ which are all located on the negative half of the real axis.

Now the residue calculus may be used to evaluate the integral in equation (10). Since the poles are all simple, the solution may be written in the form of an infinite sum

$$V(\xi,t)=R_\mathrm{o}(\xi)+\sum_{\nu=1}^{\infty}R_\nu(\xi)\exp(ts_\nu) \tag{14}$$

where R_ν is the residue of $U(\xi,s)$ at the pole s_ν. Setting $s_\nu=-1/\tau_\nu$ we obtain

$$V(\xi,t)=R_\mathrm{o}(\xi)+\sum_{\nu=1}^{\infty}R_\nu(\xi)\exp(-t/\tau_\nu) \tag{15}$$

that is, the solution is composed of a time-independent term, $R_\mathrm{o}(\xi)$, which corresponds to the steady state, and an infinite number of exponentials expiring with time.

The steady-state solution, corresponding to the pole $s_o = 0$, may be directly read off from equation (9). Because the residue of $1/s$ equals unity we have

$$R_o(\xi) = V(\xi, t = \infty) = \frac{R_j r_o I}{2(r_o + r_i)} \frac{\exp(-\xi/\lambda) - \exp(\xi/\lambda)}{(1-p)\exp(-d/2\lambda) - (1+p)\exp(d/2\lambda)}$$
$$= \frac{R_j r_o I}{2(r_o + r_i)} \frac{\sinh(\xi/\lambda)}{\sinh(d/2\lambda) + p\cosh(d/2\lambda)} \tag{16}$$

The other residues $R_\nu(\xi)$ may be calculated using conventional methods of the theory of functions.

It is easy to verify that the function defined by equation (15) satisfies the initial resting condition as well as the boundary conditions. Thus, $V(\xi, t)$ is the exact solution of the cable equation for the right half of an interior cell. Replacing ξ by $(-\xi)$ gives the solution for the left half of the cell, $-d/2 < \xi < 0$.

A point of interest is the size of the time constants of the transient terms, $\tau_\nu = -1/s_\nu = \tau_m/(b_\nu^2 + 1)$. With the parameters used in this study, the time constants are very small fractions of the membrane time constant τ_m. For example, with $R_j = 1$ MΩ, the value b_1 taken from equation (13) comes to $b_1 = 15.03$ so that $\tau_1 = \tau_m/(b_1^2 + 1) = 5.56/226.9 = 0.0245$ ms and the values τ_2, $\tau_3 \ldots$ are even smaller. Thus, for a current pulse of, say, 0.5 ms duration the voltage response of an interior cell of the fiber is practically at the steady state.

Final version accepted: August 28, 2003